iScience

CellPress
OPEN ACCESS

Article

Large-scale microRNA functional high-throughput screening identifies miR-515-3p and miR-519e-3p as inducers of human cardiomyocyte proliferation

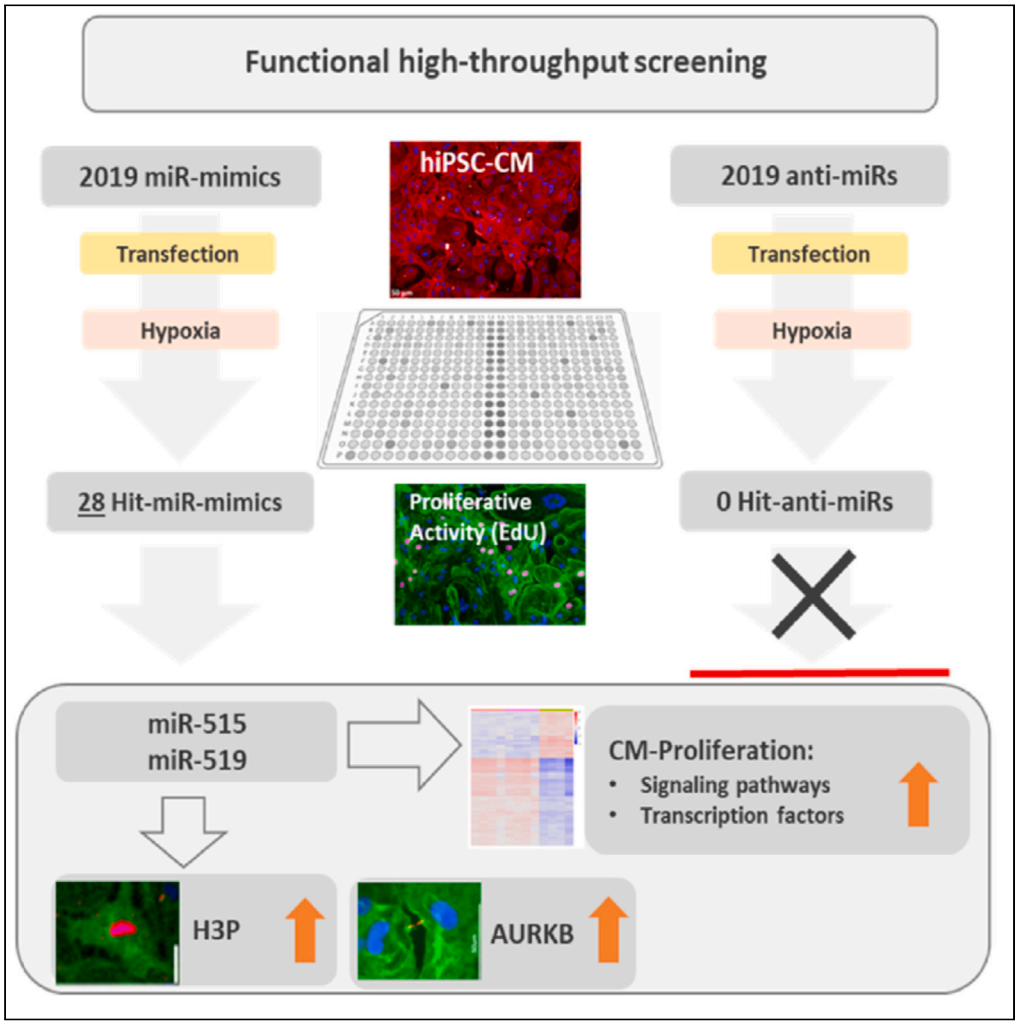

Harsha V. Renikunta, Katina Lazarow, Yiqi Gong, ..., Katrin Streckfuss-Bömeke, Ulf Landmesser, Philipp Jakob

philipp.jakob@usz.ch

Highlights

We performed the largest high-throughput screening in human iPSC-CM using 2019 miRNAs

Inhibition of individual miRNAs failed to induce proliferative activity in hiPSC-CM

In contrast, 28 miRNA-mimics substantially enhanced cell cycling in hiPSC-CM

Specifically, miR-515 and miR-519 from the C19MC induce cell division in hiPSC-CM

Renikunta et al., iScience 26, 106593
May 19, 2023
https://doi.org/10.1016/j.isci.2023.106593

iScience

CellPress
OPEN ACCESS

Article

Large-scale microRNA functional high-throughput screening identifies miR-515-3p and miR-519e-3p as inducers of human cardiomyocyte proliferation

Harsha V. Renikunta,[1,2,3] Katina Lazarow,[4] Yiqi Gong,[5] Praphulla Chandra Shukla,[1,2,6] Vanasa Nageswaran,[1,2,3,7] Hector Giral,[1,2] Adelheid Kratzer,[1,2] Lennart Opitz,[8] Felix B. Engel,[9] Arash Haghikia,[1,2,3,13] Sarah Costantino,[5] Francesco Paneni,[5] Jens Peter von Kries,[4] Katrin Streckfuss-Bömeke,[10,11,12] Ulf Landmesser,[1,2,3,13] and Philipp Jakob[1,2,3,5,13,14,*]

SUMMARY

Ischemic cardiomyopathy, driven by loss of cardiomyocytes and inadequate proliferative response, persists to be a major global health problem. Using a functional high-throughput screening, we assessed differential proliferative potential of 2019 miRNAs after transient hypoxia by transfecting both miR-inhibitor and miR-mimic libraries in human iPSC-CM. Whereas miR-inhibitors failed to enhance EdU uptake, overexpression of 28 miRNAs substantially induced proliferative activity in hiPSC-CM, with an overrepresentation of miRNAs belonging to the primate-specific C19MC-cluster. Two of these miRNAs, miR-515-3p and miR-519e-3p, increased markers of early and late mitosis, indicative of cell division, and substantially alter signaling pathways relevant for cardiomyocyte proliferation in hiPSC-CM.

INTRODUCTION

In adults, cardiac injury results in loss of cardiomyocytes and subsequent scar formation with heart failure symptoms. Despite progress made over the past decades, heart failure remains the most significant health burden worldwide. Current therapeutic approaches focus primarily on catheter-based or surgical re-perfusion strategies to minimize loss of contractile tissue as well as medical and adjunctive therapies to prevent adverse cardiac remodeling.[1]

However, potential therapies to remuscularize the heart do not exist. This lack is related to the very limited capacity of the adult heart to re-initiate cardiomyocytes turnover.[2] Therefore, human hearts are prone to hypertrophic remodeling and fibrotic scarring, resulting in heart failure with potentially reduced left ventricular ejection fraction. Intriguingly, in recent years, the dogma of the heart as a post-mitotic organ has been challenged. Studies in postnatal murine hearts and humans at young age revealed cardiomyocytes proliferation,[3,4] albeit with an excessive decline in the aged population.[2] Indeed, a small subset of cardiomyocytes retain the capacity to re-enter the cell cycle in adults that may reside preferentially in a hypoxic milieu.[5,6] These findings reveal novel opportunities to explore therapeutic strategies for cardiomyocyte regeneration in the injured myocardium. Among these, microRNAs (miRNA), a class of small non-coding RNAs, have evolved as potent modulators of cell cycling in cardiomyocytes, some of which were identified from high-throughput screenings using overexpression of miRNAs.[7–10] Indeed, exogenous downregulation,[10–13] or overexpression[7,14–18] of miRNAs have both evolved as promising strategies to induce cardiomyocyte reentry into mitotic cell cycle in neonatal and adult mouse models. However, these observations were predominantly tested in non-human models and large functional screenings using both miRNA-inhibitors and miRNA-mimics in human-induced pluripotent stem cell-derived cardiomyocytes (hiPSC-CM) have not been investigated.

Here, we tested overexpression and downregulation of 2019 miRNAs on proliferative activity in human cardiomyocytes, using hiPSC-CM. We show that individual downregulation of miRNAs is not efficient to induce cell cycle reentry. However, individual overexpression of 28 miRNAs yielded significant increase in proliferative activity in hiPSC-CM. Intriguingly, members of the human-specific C19MC cluster, miR-515-3p, and miR-519e-3p, enhance cytokinesis in human cardiomyocytes and further increase cardiomyocyte turnover after transient

[1]Deutsches Herzzentrum der Charité, Department of Cardiology, Angiology and Intensive Care, Hindenburgdamm 30, 12203 Berlin, Germany

[2]Charité – Universitätsmedizin Berlin, Corporate Member of Freie Universität Berlin and Humboldt-Universität zu Berlin, Charitéplatz 1, 10117 Berlin, Germany

[3]DZHK (German Center for Cardiovascular Research), partner site Berlin, Berlin, Germany

[4]Leibniz-Institute for Molecular Pharmacology (FMP), Campus Berlin-Buch, Robert-Rössle-Strasse 10, 13125 Berlin, Germany

[5]Center for Translational and Experimental Cardiology (CTEC), Department of Cardiology, University Hospital Zurich, University of Zurich, Wagistrasse 12, 8952 Schlieren, Switzerland

[6]School of Medical Science and Technology, Indian Institute of Technology, Kharagpur 721302, West Bengal, India

[7]Institute of Chemistry/Biochemistry, Thielallee 63, Freie Universität Berlin, 14195 Berlin, Germany

[8]Functional Genomics Center Zurich UZH/ETH, ETH Zurich and University of Zurich, 8057 Zurich, Switzerland

[9]Experimental Renal and Cardiovascular Research, Department of Nephropathology, Institute of Pathology, Friedrich-Alexander-Universität Erlangen-Nürnberg (FAU), Schwabachanlage 12 (TRC), 91054 Erlangen, Germany

Continued

hypoxia. These findings are supported by our RNA-sequencing (RNA-seq) analysis that shows substantial transcriptomic regulation of structural sarcomeric genes and activation of signaling pathways involved in proliferation and cell division after overexpression of miR-515-3p and miR-519e-3p in hiPSC-CM.

RESULTS

Transient hypoxia enhances proliferative activity in hiPSC-CM after transfection with miRNAs

We used human iPSC for differentiation into cardiomyocytes (hiPSC-CM) that were cultured for 50 to 60 days. HiPSC-CM displayed well-organized striated patterns visualized by cardiac troponin T (cTnT), and showed >90% $cTnT^+$ CM (Figure 1A). We established a liposome-based transfection method to efficiently transfect miRNAs into hiPSC-CM. Fluorescent-labeled miRNAs (FAM-miR) indicated a high incorporation after transfection into hiPSC-CM (Figure 1B). In addition, fluorescence-activated cell sorting analysis showed a high transfection efficiency in FAM-miR-transfected hiPSC-CM (Figure 1C). Furthermore, a substantial induction of a cell-death phenotype with cell shrinking and detachment was observed after transfection with silencing RNAs targeting genes for cell survival, used as a positive control for transfection efficiency (Figure S1). We used overexpression of miR-1825, a miRNA previously reported to induce proliferation in murine cardiomyocytes,[8] to test proliferative capacity in hiPSC-CM. Transfection with miR-1825-mimic increased DNA synthesis, as measured by incorporation of 5-ethynyl-2-deoxyuridin (EdU), in a dose-dependent manner (Figures 1D and 1E). Lactate dehydrogenase (LDH), a cytosolic enzyme that is released upon damage of the cell membrane and therefore quantifies cytotoxicity, was not increased after lipid-based transfection (Figure 1F). We also tested downregulation of endogenous miRNAs using anti-miRs that are known suppressors of cardiomyocyte turnover (i.e. anti-miR-99-5p, anti-miR-100-5p,[13] and anti-miR-195-5p[11]). Expression of endogenous miRNAs was substantially downregulated after anti-miR transfection, as shown for miR-195-5p (Figure 1G). Indeed, anti-miR-99-5p and anti-miR-195-5p significantly induced proliferative activity in hiPSC-CM as assessed by EdU incorporation (Figure 1H). In addition, Western blot analysis revealed downregulation of cyclin-dependent kinase inhibitor 1A (CDKN1A), an important cell cycle inhibitor, in hiPSC-CM treated with anti-miR-195 (Figure 1I). These results convincingly show that lipid-based transfection of miR-mimic and anti-miRs efficiently induce cell cycle reentry in hiPSC-CM. In order to explore miRNA modulation in a hypoxic milieu, that is present in patients with myocardial infarction, we exposed hiPSC-CM to transient hypoxia (0.5% O2). Interestingly, transient hypoxia further increased EdU incorporation in miR-1825-transfected hiPSC-CM that was not observed after miR-scrambled transfection (Figure 1J). These findings prompted us to use this model for investigating proliferative activity in hiPSC-CM by using a library of 2019 miR-mimics and anti-miRNAs.

Selective overexpression of miRNAs induces proliferative activity in hiPSC-CM

We performed a functional high-throughput screening by using a miRNA library (Ambion; mirVana Human Library v19.0). Two thousand and nineteen miR-mimics were individually transferred to 384-wells pre-plated with hiPSC-CM. HiPSC-CM were transiently exposed to hypoxia for 2 h. Using a high-content imaging system, enhanced cell cycle activity of miRNA-transfected hiPSC-CM was assessed by EdU incorporation (Figure 2, Table S1, Figure S2). *Z* score, a normalizing method, was calculated for each candidate miRNA on the plate by subtracting all candidate wells in the plate and dividing the difference by median absolute deviation of all candidate wells in the plate. Transfection of miRNA-mimics identified 40 miRNAs that reached significant levels of cell cycle reentry in hiPSC-CM (*Z* score >3) (Figures 2A–2D). Twenty-eight miRNAs substantially increased number of EdU-positive hiPSC-CM in both replicates (Figure 2C, Table S2). We validated proliferative activity in a hit-picking screening, where these 28 miRNAs were assessed separately (Figure 2E). Interestingly, several miRNA-mimics identified in the high-throughput screening are members of miRNA-families, such as miR-148a-3p/miR-148b-3p (miRNA-148 family) and miR-212-3p/miR-132-3p (miRNA-212 family). In addition, five candidate miRNAs belong to the chromosome 19 miR-cluster (C19MC, hsa-miR-515-3p, hsa-miR-519e-3p, and hsa-miR-517c-3p) and adjacent miR-371-373 cluster (hsa-miR-371a-3p and hsa-miR-371b-3p), located on chromosome 19q13.41.[19,20] This primate-specific imprinted cluster is not detected in the human heart muscle[21] (Figure S3), but predominantly expressed in the placenta and in undifferentiated cells,[19,22] and experimental studies have investigated members of this cluster in the context of differentiation, invasion, and proliferation in different cell types of the placenta.[23,24] As these biological features regulated by miRNAs of C19MC are highly relevant for cardiac regeneration, we further focused our study on miR-515-3p, miR-519e-3p, and miR-371a-3p that showed the highest proliferative activity within these clusters (Figures S4A, S4B, and Table S3).

[10]Clinic for Cardiology and Pneumology, University Medical Center Göttingen, Robert-Koch-Strasse 40, 37075 Göttingen, Germany

[11]DZHK (German Center for Cardiovascular Research), partner site Göttingen, Robert-Koch-Strasse 42a, 37075 Göttingen, Germany

[12]Institute of Pharmacology and Toxicology, University of Würzburg, Versbacher Str. 9, 97078 Würzburg, Germany

[13]Berlin Institute of Health (BIH) at Charité – Universitätsmedizin Berlin, Charitéplatz 1, 10117 Berlin, Germany

[14]Lead contact

*Correspondence: philipp.jakob@usz.ch

https://doi.org/10.1016/j.isci.2023.106593

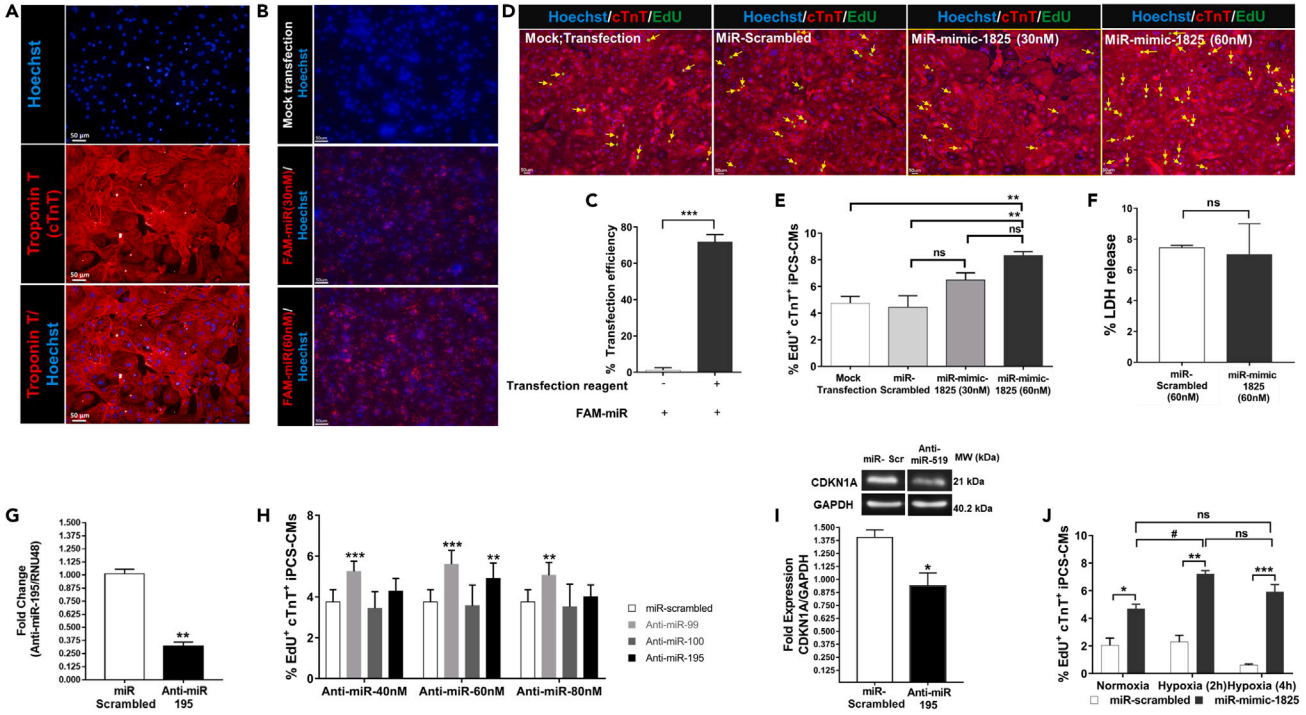

Figure 1. Transient hypoxia increases miRNA-induced proliferative potential in hiPSC-CM

(A) HiPSCs were generated from skin fibroblasts and differentiated into cardiomyocytes (hiPSC-CM). Immunofluorescence images showing Hoechst (blue, nuclei) and cardiac troponin T (red)-positive hiPSC-CM.

(B) Representative images of mock-transfected (top image) and fluorescently labeled pre-miRNA (FAM-miR) transfected hiPSC-CM at 24 h post transfection (30 nM, middle; 60 nM lower image).

(C) Transfection efficiency as analyzed by FACS analysis (n = 3 biological replicates); ***p < 0.001.

(D and E) Representative immunofluorescence images and (E) quantification of EdU uptake in mock-transfected hiPSC-CM, and after transfection with miRNA-scrambled, miR-mimic-1825 (30 nM), and miR-mimic-1825 (60 nM). Hoechst (blue, nuclei), cardiac troponin T (red) and EdU (green); arrows pointing to EdU-positive hiPSC-CM (n = 3 biological replicates); **p < 0.01.

(F) Lactate dehydrogenase (LDH) release of hiPSC-CM after transfection with miR-scrambled and miR-mimic-1825 (60 nM). Supernatants were collected 24 h post transfection (n = 3 biological replicates).

(G) MiRNA expression in hiPSC-CM after transfection with miR-scrambled or anti-miR-195-5p 48 h post transfection (n = 4 biological replicates); **p < 0.01.

(H) Incorporation of EdU in hiPSC-CM after transfection with miRNA-scrambled, anti-miR-99-5p, anti-miR-100-5p, and anti-miR-195-5p (concentrations: 40 nM, 60 nM, and 80 nM). EdU-positive hiPSC-CM were assessed 96 h post transfection (n = 3 biological replicates); **p < 0.01; ***p < 0.001 vs. miR-scrambled.

(I) Representative Western blots (top) and quantification of CDKN1A derived from lysates of hiPSC-CM after transfection with miR-scrambled or anti-miR-195-5p 72 h post transfection (n = 4 biological replicates); *p < 0.05.

(J) Incorporation of EdU in hiPSC-CM transfected with miR-scrambled or miR mimic-1825 under normoxia or after transient hypoxia for 2 and 4 h (n = 3 biological replicates); *p < 0.05 miR-scrambled vs. miR-mimic-1825; #p < 0.05 miR-mimic-1825 normoxia vs. hypoxia (n = 3 biological replicates). Scale bar = 50 μm. 50- to 60-days-old hiPSC-CM were used for experiments.

Selective inhibition of miRNAs is not sufficient to induce a proliferative response in hiPSC-CM

We next assessed downregulation of 2019 miRNAs in hiPSC-CM on their proliferative effects (Figures 3A–3D and Table S4). We individually transfected 2019 anti-miRs into hiPSC-CM that were exposed to transient hypoxia for 2 h. Notably, two miRNA-inhibitors significantly induced proliferative activity (*Z* score >3 in both replicates) (Figures 3B–3D, Table S5, Figure S5). However, the increase of EdU-positive cardiomyocytes was modest (anti-miR-let-7c-5p: 6.69 ± 0.8%, anti-miR-365a-3p: 6.15 ± 0.6%) and validation of these candidates in a second screening, where anti-miR-let-7c-5p and anti-miR-365a-3p were assessed separately, did not show a substantial increase in EdU uptake as compared to mock-transfected hiPSC-CM (Figure 3E). Conclusively, as compared to the miR-mimic screening, induction of proliferative capacity after anti-miR transfection was not sufficient for cell cycle reentry in hiPSC-CM (Figure 3F; anti-miR screen from Figure 3C (blue circles) and miR-mimic screen from Figure 2C (gray and red circles) are shown for comparison). Therefore, we focused our study on candidate miRNAs derived from the miR-mimic screening (miR-mimic-515-3p, miR-mimic-519e-3p, and miR-mimic-371a-3p).

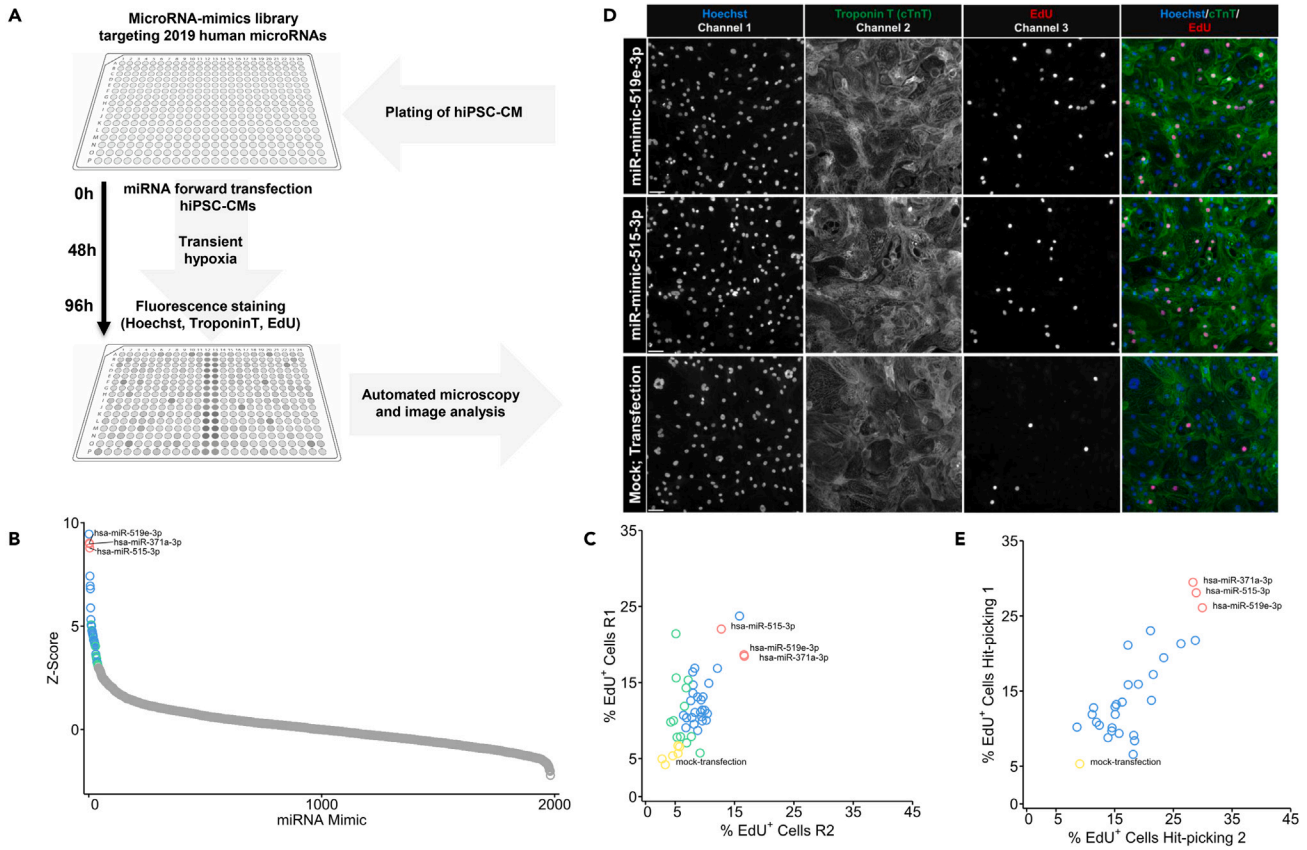

Figure 2. Functional high-throughput screening of 2019 miR-mimics identifies 28 miRNAs that induce proliferative activity in hiPSC-CM

(A) Graphical illustration of the functional high-throughput (HTS) screening workflow. A miRNA-library was used for overexpression of 2019 miRNAs (miR-mimics). HTS was performed in duplicates.

(B) EdU incorporation in hiPSC-CM was assessed after individual transfection with 2019 miRNA-mimics. Sigma plot indicates distribution of mean Z-scores (mean of two replicates) for the 2019 miRNA-mimics tested. Candidates with a *Z* Score >3 in both replicates are indicated in blue or highlighted in red, candidates with a *Z* score >3 in one of the replicate are highlighted in green. Blue, red, and green circles delineate a significant increase in EdU uptake.

(C) Forty miR-mimics significantly increased EdU uptake in hiPSC-CM in the HTS. The data points indicate percentage of EdU incorporation in hiPSC-CM in both the replicates. Red colored data points highlight the top candidates derived from the screening.

(D) Immunofluorescence images of hiPSC-CM showing Hoechst (blue, nuclei), cardiac troponin T (green), and EdU (red) after transfection with miR-mimic-519e-3p, miR-mimic-515-3p, and mock transfection.

(E) Twenty-eight candidate miRNAs with *Z* score >3 in both replicates were retested in a hit-picking screening. Shown is the mean EdU uptake of two screens. The data points indicate percentage of EdU-incorporation of hiPSC-CM in both the replicates. Scale bar = 50 μm. 50- to 60-days-old hiPSC-CM were used for experiments.

MiR-515-3p, miR-519e-3p, and miR-371a-3p substantially induce proliferation in hiPSC-CM

First, in order to define efficacy and toxicity, miR-mimic-515-3p, miR-mimic-519e-3p, and miR-mimic-371a-3p were transfected with increasing concentrations. Transfection with miR-mimic (60 nM) induced proliferative activity significantly above lower concentrations, whereas higher concentrations did not further increase cardiomyocyte turnover (Figures 4A and 4B). Importantly, miR-mimic (60 nM) transfection did not affect toxicity, as assessed by LDH assay (Figure 4C). Of note, transfection of hsa-miR-590-3p, previously reported to induce cardiomyocyte proliferation in murine cardiomyocytes,[8,18] did not result in enhanced EdU incorporation in hiPSC-CM (Figure 4A). We next tested if transient hypoxia, as observed for miR-mimic-1825, is critical for proliferative activity in hiPSC-CM. Interestingly, transfecting hiPSC-CM with miR-515-3p, miR-519e-3p not only substantially increased proliferation in normoxic conditions but also further increased EdU uptake in hiPSC-CM after transient hypoxia. Of note, this effect was not observed in miR-scrambled or miR-371a-3p-mimic-transfected hiPSC-CM (Figure 4D, 4E, S6A, and S6B). Furthermore, we analyzed phospho-histone H3 (H3P), a marker of late G2 mitosis (Figure 5). Transfection with miR-515-3p, miR-519e-3p, and miR-371a-3p-mimic increased number of H3P-positive hiPSC-CM as compared to miR-scrambled-treated hiPSC-CM. In addition, a transient period of hypoxia (2 h), as

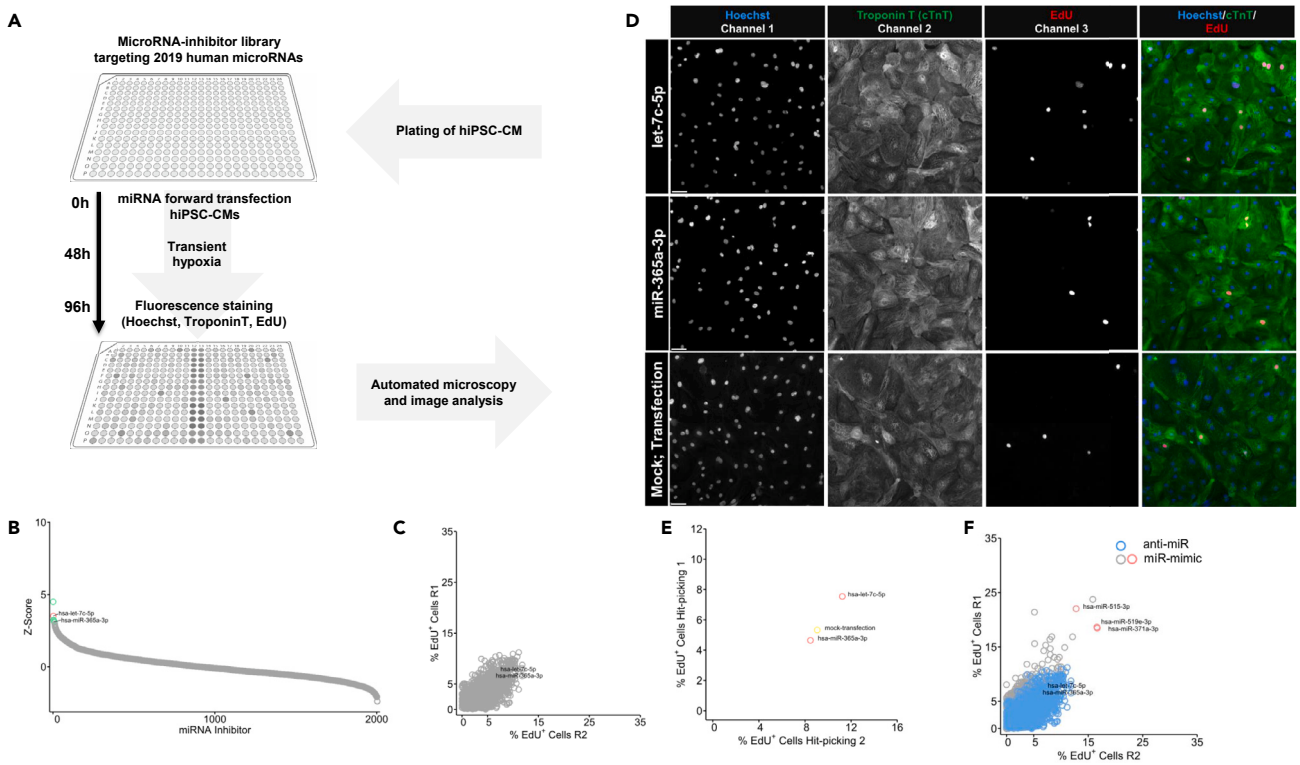

Figure 3. Individual transfection of 2019 miRNA-inhibitors (anti-miRs) fails to induce proliferation in hiPSC-CM

(A) Graphical illustration of the HTS workflow. A miRNA-library was used for inhibition of 2019 miRNAs (anti-miRs). HTS was performed in duplicates.

(B) EdU incorporation into hiPSC-CM was assessed after individual transfection with 2019 anti-miRs. Sigma plot indicates distribution of mean Z-scores (mean of two replicates) for the 2019 anti-miRs. A *Z* score >3 in both replicates, indicated by red and green circles, was used to delineate a significant increase in EdU uptake.

(C) Two out of 2019 anti-miRs, namely anti-let-7c-5p and anti-miR-365a-3p significantly increased EdU uptake in hiPSC-CM. The data points indicate percentage of EdU incorporation of hiPSC-CM in both the replicates.

(D) Immunofluorescence images of hiPSC-CM showing Hoechst (blue, nuclei), cardiac troponin T (green), and EdU (red) after transfection with anti-let-7c-5p, anti-miR-365a-3p, and mock transfection.

(E) Anti-let-7c-5p and anti-miR-365a-3p were retested in duplicate. Shown is the mean EdU uptake of two screens.

(F) Anti-miR HTS from Figure 3C (blue circles) and miR-mimic HTS from Figure 2C (gray and red circles) are shown for comparison to illustrate that transient downregulation of miRNA using anti-miRs is not effective to induce proliferative capacity as compared to miR-mimics. Scale bar = 50 μm. 50- to 60-days-old hiPSC-CM were used for experiments.

compared to normoxia, increased the number of H3P-positive hiPSC-CM in miR-519e-3p-mimic and miR-515-3p-mimic-transfected hiPSC-CM but not after transfection with miR-371a-3p-mimic (Figures 5A, 5B, S7A, and S7B). With respect to potential gender differences, we observed similar capacity of candidate miR-mimics to induce proliferation in hiPSC-CM derived from female and male donors (Figure S8). We also performed H3P staining over a period of five days to understand whether miRNA-induced increase in mitosis is persistent. Herein, we observed a peak at day three post transfection, suggesting a brief proliferative burst after lipid-based miRNA transfection (Figure S9).

These results indicate that miR-515-3p, miR-519e-3p, and miR-371a-3p are robust inducers of cardiomyocyte proliferation. However, transient hypoxia did not result in an enhanced cardiomyocytes turnover after miR-371a-3p overexpression. As this may be relevant in a hypoxic milieu that is present in patients with myocardial infarction, we further focused our study on miR-515-3p and miR-519e-3p.

MiR-515-3p and miR-519e-3p markedly alter expression of genes relevant for dedifferentiation and proliferation

Cardiomyocyte proliferation involves regulation of genes that are necessary for cell cycle reentry. Therefore, we assessed gene expression of positive and negative cell cycle regulators after transfection of hiPSC-CM with miR-515-3p and miR-519e-3p (Figure 6). First, we confirmed, as already observed in HEK

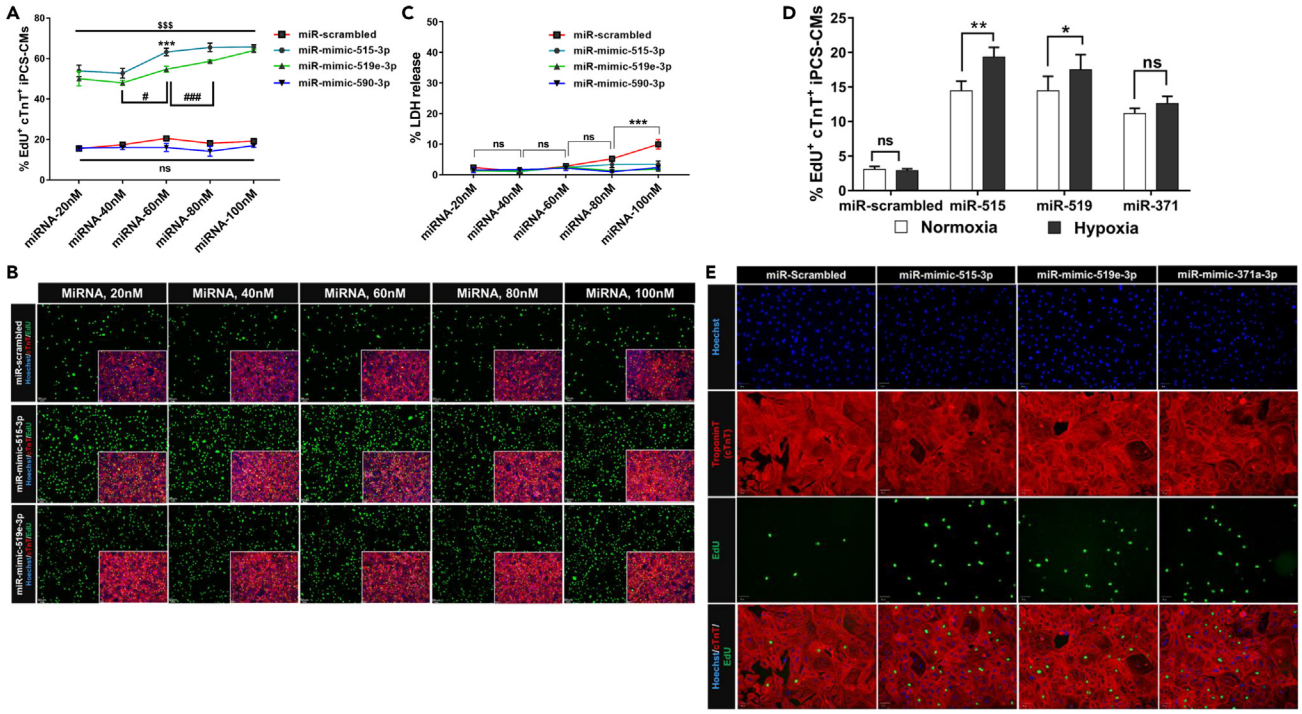

Figure 4. Overexpression of hsa-miR-515-3p, hsa-miR-519e-3p, and hsa-miR-371a-3p increase EdU uptake without affecting cytotoxicity in hiPSC-CM

(A) Incorporation of EdU in hiPSC-CM after transfection with increasing miR-mimic concentrations (20, 40, 60, 80, and 100 nM). MiR-scrambled and miR-mimic-590-3p were used as controls. EdU-positive hiPSC-CM were assessed 96 h post transfection (n = 3 biological replicates); $, miR-scrambled (20–100 nM) vs. miR-mimic-515-3p and miR-mimic-519e-3p (20–100 nM); ns, miR-scrambled vs. miR-590-3p (20–100 nM); *, miR-mimic-515-3p between different miRNA-concentrations (20–100 nM). #, miR-mimic-519e-3p between different miRNA-concentrations (20–100 nM); #p < 0.05; ***, $$$, ###p < 0.001.

(B) Representative immunofluorescence images of hiPSC-CM showing EdU (green); insets represent merged images of Hoechst (blue, nuclei), cardiac troponin T (red), and EdU (green).

(C) Analysis of cytotoxicity, as assessed by LDH release, of hiPSC-CM transfected with different miRNA-mimic concentrations. Supernatants were collected 24 h post transfection. Only miR-scrambled (100 nM) increased toxicity in hiPSC-CM (n = 3 biological replicates); ***p < 0.001.

(D) EdU uptake in hiPSC-CM under normoxia or transient exposure to hypoxia (2 h, 0.5% O2) after transfection with miR-scrambled, miR-mimic-515-3p, miR-mimic-519e-3p, and miR-mimic-371a-3p (n = 3 biological replicates); *p < 0.05, **p < 0.01.

(E) Representative immunofluorescence images of hiPSC-CM after transfection with miR-scrambled, miR-mimic-515-3p, miR-mimic-519e-3p, and miR-mimic-371a-3p and transient hypoxia. Hoechst (blue), cardiac troponin T (red), and EdU (green). Scale bar = 50 μm. Forty-five to 50 days (Figures 4A–4C), and 55- to 60-days (Figures 4D and 4E)-old hiPSC-CM were used for experiments.

293 cells,[25] a substantial suppression of CDKN1A in hiPSC-CM both by RT-qPCR (Figure 6A) and immunofluorescence imaging (Figure 6B). Similarly, downregulation of CDKN1B was observed (Figure 6C), whereas CDKN1C was not significantly reduced (Figure 6D). Moreover, genes that restrain cell cycle progression within the Hippo-signaling pathway, LATS1 and MOB1B, were significantly downregulated after miR-515-3p and miR-519e-3p-mimic transfection (Figures 6E and 6F). Importantly, miR-515-3p and miR-519e-3p-transfected hiPSC-CM showed a substantial increase in cyclin A2 (CCNA2) expression, a key regulator of cell cycle progression through G1/S and G2/M phase.[26,27] In addition, the cell cycle activator cyclin B1[28,29] was markedly upregulated, whereas cyclin D2[30,31] did not show a differential expression (Figures 6G–6I). In line, sarcomeric genes that are involved in structural maturation, such as myosin light chain-2, myosin light chain-7, and myomesin 3, were markedly downregulated (Figures 6J–6M). We also investigated members of the pocket protein family of tumor suppressors, namely RB transcriptional corepressor 1 (Rb1) and RB transcriptional corepressor like 2 (Rbl2) that are upregulated upon differentiation and suppress cell cycle activators and Rbl1 that is downregulated in adult cardiomyocytes.[32–34] Herein, a marked downregulation of Rb1 and Rbl2 and upregulation of Rbl1 was detected after miR-mimic-515-3p transfection (Figures 6N–6P). Next, we validated our findings on protein level by conducting Western blots (Figure 6Q–6T). After transfection of miR-515-3p and miR-519e-3p in hiPSC-CM, a marked downregulation of CDKN1A and upregulation of CCNA2 on protein level was confirmed (Figures 6R and 6S). In addition, we

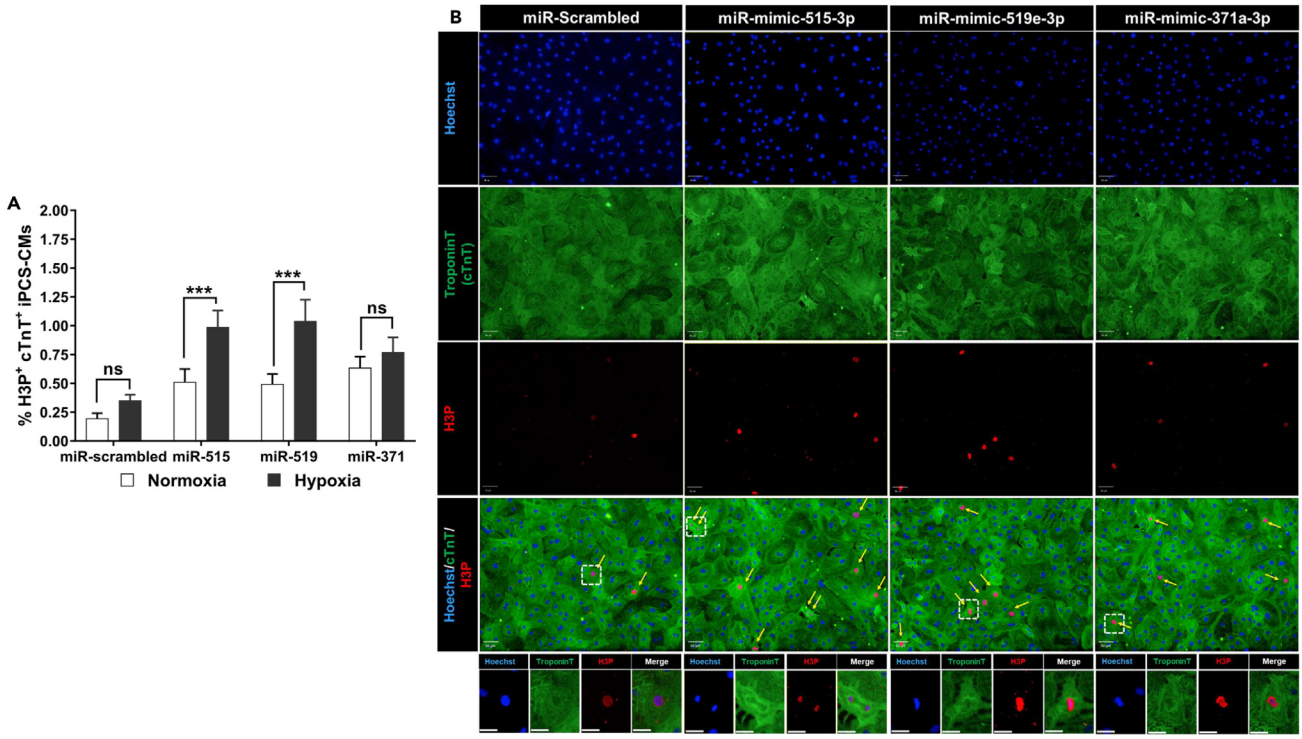

Figure 5. Overexpression of hsa-miR-515-3p, hsa-miR-519e-3p, and hsa-miR-371a-3p induce mitosis in hiPSC-CM

(A) Analysis of mitosis in hiPSC-CM, as assessed using phospho-histone H3 (H3P). H3P-positive hiPSC-CM under normoxia or transient exposure to hypoxia (2 h, 0.5% O2) after transfection with miR-scrambled, miR-mimic-515-3p, miR-mimic-519e-3p, and miR-mimic-371a-3p (n = 5 biological replicates); ***$p < 0.001$.

(B) Representative immunofluorescence images of hiPSC-CM after transfection with miR-scrambled, miR-mimic-515-3p, miR-mimic-519e-3p, and miR-mimic-371a-3p and transient hypoxia. Arrows pointing to H3P-positive hiPSC-CM. Magnification of insets below. Hoechst (blue, nuclei), cardiac troponin T (green), and H3P (red). Scale bar = 50 μm. 50- to 60-days-old hiPSC-CM were used for experiments.

observed a substantial increase of Aurora B-kinase, a midbody-associated protein marker needed for completion of cell division (Figure 6T). In conclusion, overexpression of miR-515-3p and miR-519e-3p substantially reduce expression of genes related to mitotic arrest and significantly upregulate genes involved in cell cycle reentry.

MiR-515-3p and miR-519e-3p markedly increase mitosis and cell division

For identification of hiPSC-CM undergoing cytokinesis after miR-515-3p, miR-519e-3p, and miR-scrambled transfection, we visualized Aurora B-kinase. Herein, we were able to differentiate all stages of late mitosis, including movement of Aurora B-kinase to the midbody in cytokinesis (Figure 7A). In addition, miR-515-3p and miR-519e-3p-treated hiPSC-CM showed disorganization of sarcomere structures (Figure 7B). Importantly, the number of hiPSC-CM in prophase or stages of late mitosis was substantially increased after miR-515-3p and miR-519e-3p transfection, as indicated by Aurora B-kinase positive nuclei (Figure 7C). We also observed a substantially higher number of hiPSC-CM positive for localization of Aurora B-kinase in the midbodies, suggestive of cytokinesis after treatment with miR-515-3p and miR-519e-3p (Figures 7D and 7E). In conclusion, miR-515-3p and miR-519e-3p substantially induce early and late stages of mitosis and cell division.

Transcriptome analysis after overexpression of miR-515-3p and miR-519e-3p in hiPSC-CM reveals substantial changes on structural organization and proliferation pathways

To further understand pathways involved in the observed miRNA-induced regenerative potential, we performed RNA-seq after overexpression of miR-515-3p and miR-519e-3p in hiPSC-CM (Figure 8). The majority of genes modulated by miR-515-3p and miR-519e-3p are overlapping, as expected given the origin of the same miRNA family (Figures 8A and 8B). Further analysis identified two major gene clusters (Figure 8C). We

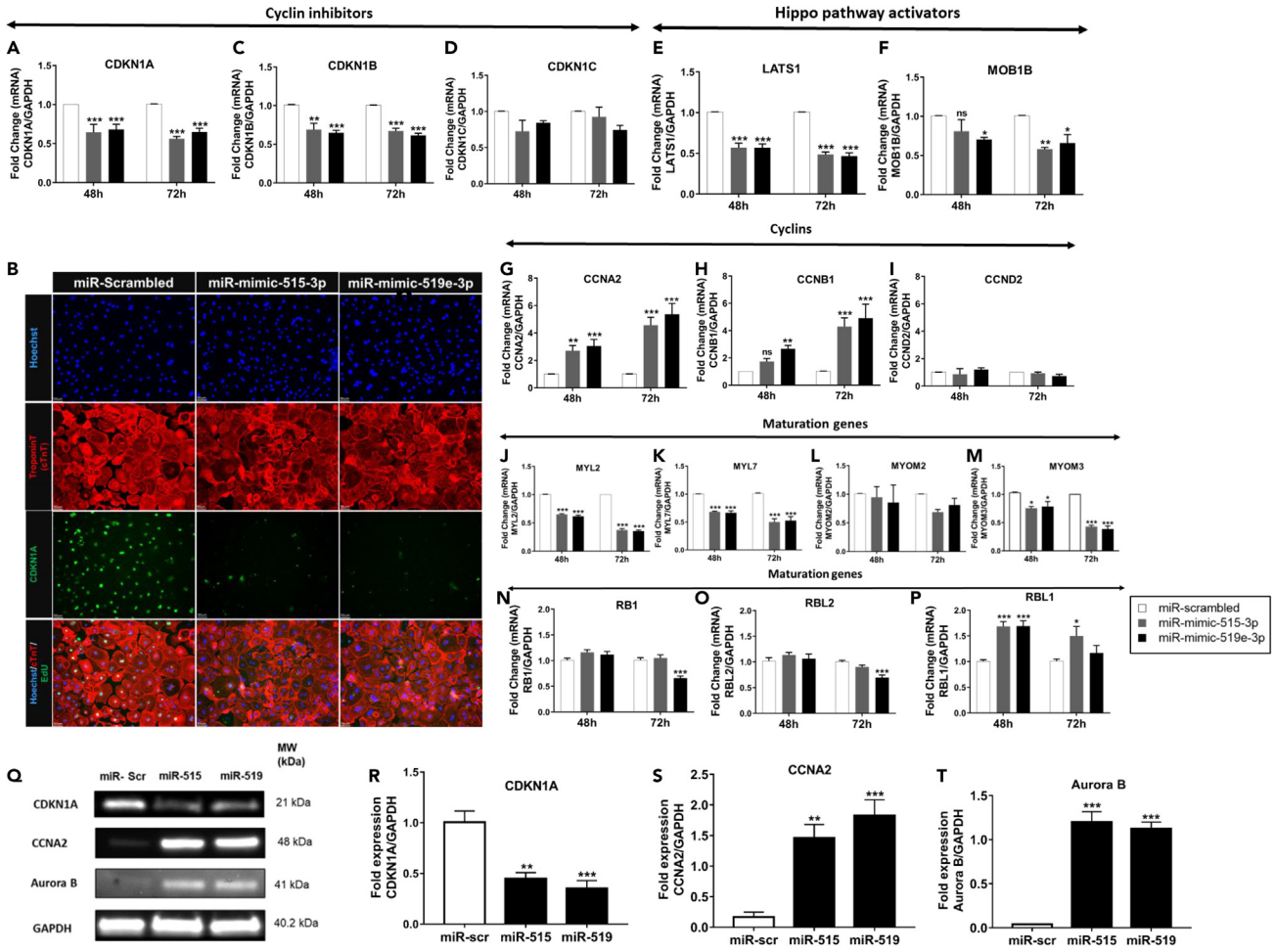

Figure 6. Overexpression of hsa-miR-515-3p and hsa-miR-519e-3p in hiPSC-CM modulates genes involved in cardiomyocyte dedifferentiation and proliferation

(A, C–M) HiPSC-CM were transfected with miR-scrambled, miR-mimic-515-3p, and miR-mimic-519e-3p for 24 h. RNA was isolated 48 and 72 h post transfection to perform qRT-PCR. (A) Cell cycle inhibitor *CDKN1A* (n = 4 biological replicates), (B) Representative immunofluorescence images of CDKN1A in hiPSC-CM after transfection with miR-scrambled, miR-mimic-515-3p, and miR-mimic-519e-3p. Hoechst (blue, nuclei), cardiac troponin T (red), and CDKN1A (green). (C and D) *CDKN1B and CDKN1C*. (E and F) Hippo pathway activators (LATS1 and MOB1B). (G–I) Cell cycle activators *(CCNA2, CCNB1, and CCND2);* (6C-6I, n = 4 biological replicates). (J–M) Sarcomeric genes involved in maturation (*MYL2, MYL7, MYOM2, and MYOM3*) (n = 4–5 biological replicates); (N–P) Retinoblastoma (Rb) pocket genes *Rb1*, *Rbl2*, and *Rbl1* (n = 3 biological replicates); *p < 0.05, **p < 0.01, ***p < 0.001 vs. miR-scrambled. (Q) Representative Western blots and quantification of (R) CDKN1A, (S) CCNA2, and (T) Aurora B-kinase derived from lysates of hiPSC-CM after transfection with miR-scrambled, miR-mimic-515-3p, and miR-mimic-519e-3p for 24 h. Protein lysates were analyzed at 72 h post transfection (n = 3–4 biological replicates); *p < 0.05, **p < 0.01, ***p < 0.001 vs. miR-scrambled. Scale bar = 50 μm. 50- to 60-days-old hiPSC-CM were used for experiments.

used gene ontology (GO) enrichment analysis to investigate whether specific GO terms are associated with differentially expressed genes in the clusters (Figure 8D). Downregulated genes are strongly involved in structural and sarcomeric organization (Figure 8D, left). In contrary, upregulated enriched GO terms comprise processes involved in DNA replication, cell cycle, and cell division (Figure 8D, right). Notably, key signaling pathways regulating cardiomyocytes proliferation, such as the PI3K-Akt, the WNT/B-catenin, and TGF-B/SMAD (Figures 8E–8G), were enriched in miR-mimic-transfected hiPSC-CM. Moreover, we observed that Notch, Hippo/YAP, and NRG/ERBB signaling pathways showed a trend toward significant enrichment after miR-mimic overexpression (Figures 8H–8J). In addition, we analyzed transcription factors that are differentially regulated (Figure 8K). Interestingly, several cell cycle-related transcription factors from the E2F family (E2F1, E2F2, and E2F7), the MYB transcription factor family (MYBL1 and MYBL2), and FOXM1 were upregulated upon miR-mimic transfection (Figure 8K). As we observed an increase in proliferation after miR-mimic transfection and transient hypoxia as compared to normoxia, we also investigated

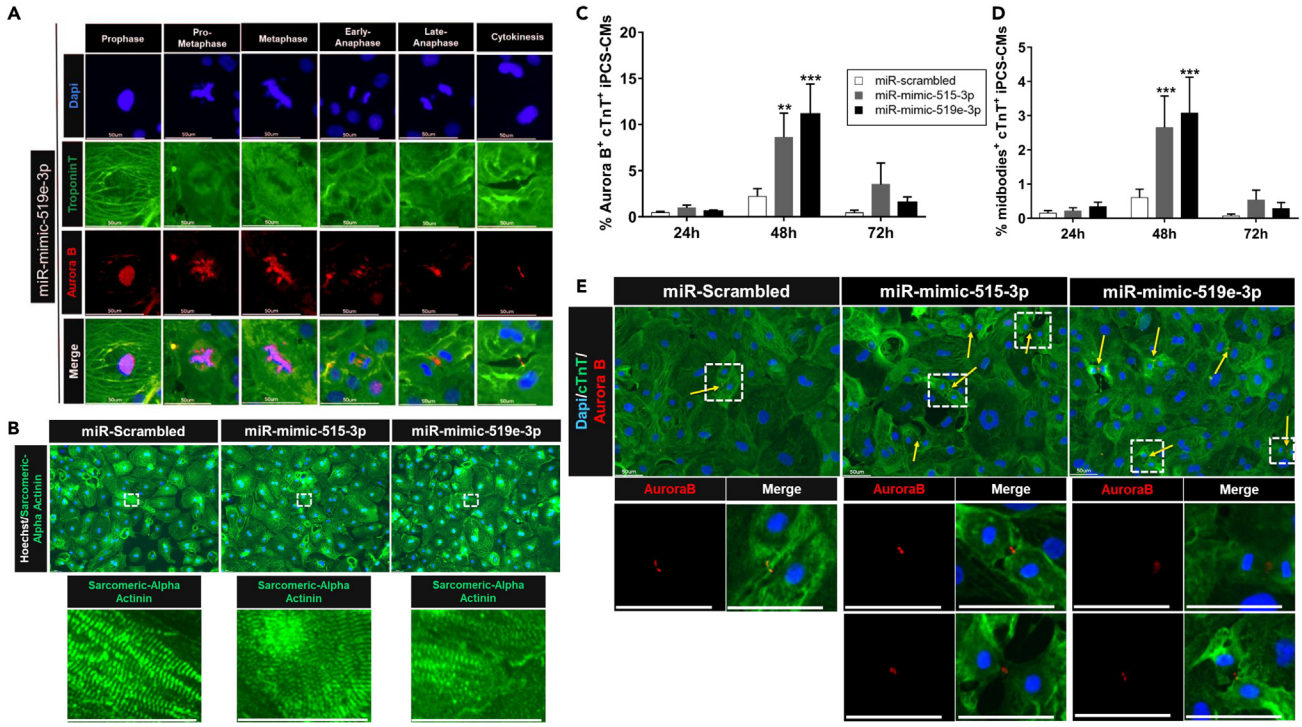

Figure 7. Overexpression of hsa-miR-515-3p and hsa-miR-519e-3p induce cytokinesis in hiPSC-CM

(A) Representative immunofluorescence images of Aurora B-kinase localization in different phases of mitosis after transfection with miR-mimic-519e-3p. Dapi (blue, nuclei), cardiac troponin T (green), and Aurora B-kinase (red). HiPSC-CM were assessed 48 h post transfection.

(B) Representative immunofluorescence images for illustration of sarcomeric disassembly in hiPSC-CM after transfection with miR-mimic-515-3p and miR-mimic-519e-3p. Hoechst (blue, nuclei), sarcomeric alpha-actinin (green).

(C) Analysis of Aurora B-kinase-positive hiPSC-CM after transfection with miR-scrambled, miR-mimic-515-3p, and miR-mimic-519e-3p (n = 4 biological replicates); **p < 0.01; ***p < 0.001 vs. miR-scrambled.

(D) Analysis of midbodies as assessed with Aurora B-kinase after transfection with miR-scrambled, miR-mimic-515-3p, and miR-mimic-519e-3p (n = 4 biological replicates). ***p < 0.001 vs. miR-scrambled.

(E) Representative immunofluorescence images of hiPSC-CM after transfection with miR-scrambled, miR-mimic-515-3p, and miR-mimic-519e-3p for quantification of Aurora B-kinase. Arrows pointing to hiPSC-CM undergoing cytokinesis. Dapi (blue, nuclei), cardiac troponin T (green), and Aurora B-kinase (red). Scale bar = 50 μm. 50- to 60-days-old hiPSC-CM were used for experiments.

enrichment of GO terms in the context of hypoxia. Indeed, genes relevant for response to hypoxia were significantly enriched in miR-mimic-treated hiPSC-CM (Figure 8L). Collectively, these findings suggest that the proliferative potential of miR-515-3p and miR-519e-3p is mediated by a broad panel of genes that de-repress inhibited proliferative pathways relevant for cardiomyocytes proliferation and cell division.

DISCUSSION

Our findings here provide evidence that overexpression of miRNAs is effective to induce proliferation in human iPSC-CM. We have tested overexpression and inhibition of more than two thousand miRNAs in hiPSC-CM using functional high-throughput screenings. Whereas downregulation of miRNAs did not robustly enhance cell cycle reentry, 28 out of 2019 miRNA-mimics significantly increased proliferative activity in hiPSC-CM. Derived from the high-throughput screening, we validated two miRNA members of the primate-specific C19MC cluster, miR-515-3p and miR-519e-3p. These miRNAs substantially increased markers of early and late mitosis in hiPSC-CM, indicative of cell division. Intriguingly, these miRNAs exert additive proliferative effects in hiPSC-CM upon transient hypoxia that was not observed with other candidate miRNAs, such as miR-371a-3p. These findings suggest that miR-515-3p and miR-519e-3p are potential attractive targets for induction of cardiomyocyte proliferation in a transient hypoxic milieu, such as present in myocardial infarction.

Strategies to induce cardiomyocyte proliferation evolve as a novel therapeutic option in adults, as emerging evidence showed that cardiomyogenesis is not restricted to embryonic stages. Studies in mice and humans have shown that cardiomyocyte turnover persists in postnatal mice and humans in adolescence.[2,4–6,12,35] However, this

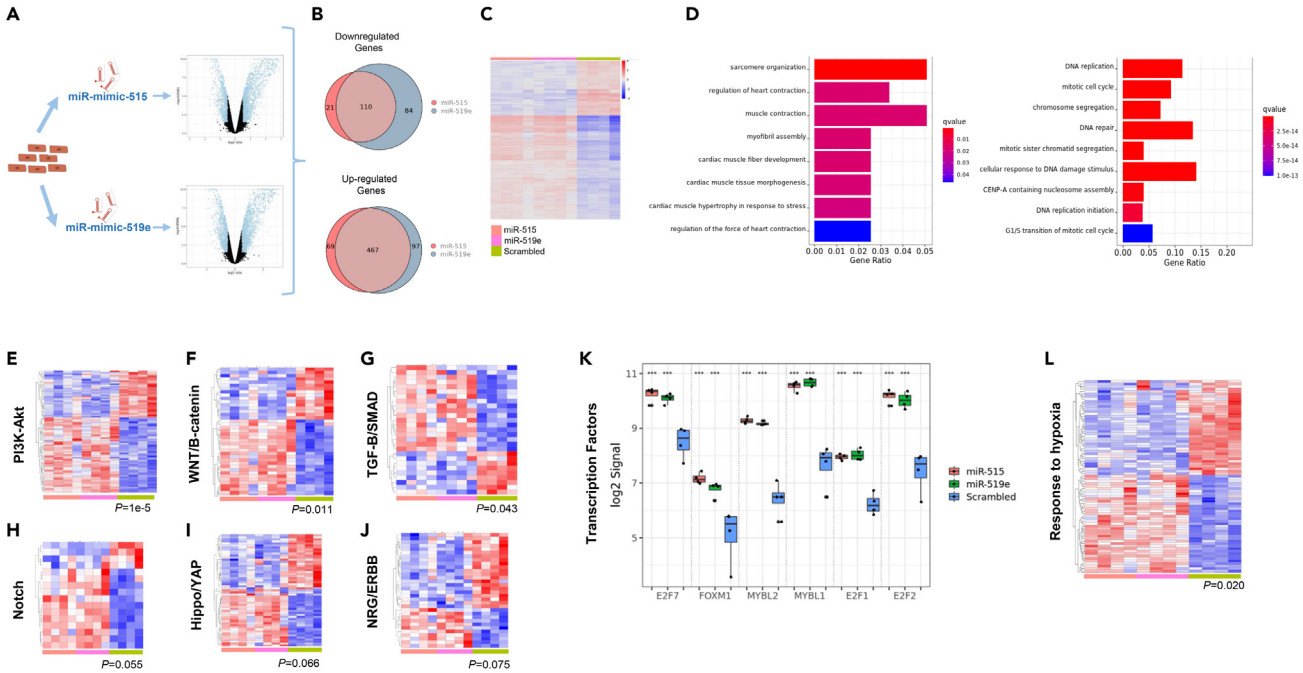

Figure 8. RNA-seq reveals a substantial modulation of biological processes involved in cardiomyocyte proliferation after miR-515-3p and miR-519e-3p overexpression in hiPSC-CM

HiPSC-CM were treated with scrambled-miRNA (Scrambled), miR-mimic-515-3p (miR-515), and miR-mimic-519e-3p (miR-519) (n = 4 biological replicates per group). RNA was isolated and subjected to RNA-seq.

(A and B) Volcano plots and (B) Euler diagram show overlapping and differentially expressed genes in hiPSC-CM after miR-mimic-515-3p and miR-mimic-519e-3p treatment as compared to miR-scrambled transfected hiPSC-CM. False discovery rate (fdr) < 0.05 and |log2 fold change| > 1 were used for candidate selection.

(C) Heatmap, arranged by hierarchical clustering of differentially expressed genes (miR-mimic-515-3p (left rows), miR-mimic-519e-3p (middle rows), and miR-scrambled (right rows). The color represents the relative expression level (log2 scaled FPKM). Red, increased expression; blue: reduced expression.

(D) Two clusters were identified after miR-mimic-515-3p and miR-mimic-519e-3p as compared to miR-scrambled transfection in hiPSC-CM. Enriched gene ontology (GO) terms of downregulated (left) and upregulated (right) genes, ordered from top to bottom by p value.

(E–J) Shown are differentially expressed genes (fdr <0.05) of signaling pathways involved in cardiomyocyte proliferation. P values for representative pathways are shown on lower right of the heat maps.

(K) Analysis of transcription factors related to cardiomyocyte proliferation that are significantly upregulated after miR-mimic-transfection in hiPSC-CM. ***p < 0.001.

(L) Gene ontology analysis for differentially expressed genes (fdr <0.05) in response to hypoxia (GO:0070482) after miR-mimic-transfection in hiPSC-CM. 50- to 60-days-old hiPSC-CM were used for experiments.

reparative potential declines over the years with a very low number of cardiomyocytes undergoing cell cycle reentry in adults that are the most vulnerable to myocardial injury.[2,4]

In this regard, miRNA-targeted therapies have the potential to reinforce turnover of preexisting cardiomyocytes. Several experimental studies have shown that downregulation of endogenous miRNAs increase proliferation *in vitro* and *in vivo* in murine models.[10–13] Conversely, our high-throughput screening did not identify miRNA-inhibitors as inducers of cell cycle reentry in hiPSC-CM. Transfection of anti-let-7c that has been shown to increase turnover of murine cardiomyocytes *in vivo*,[13] increased EdU uptake in the initial screening but failed in the validation screening. The absence of a significant proliferative response of the 2019 investigated miRNA-inhibitors can be related to inter-species differences or to the single lipid-based miRNA transfection used in our screening. If prolonged downregulation of endogenous miRNAs via adeno-associated virus may enhance proliferation in human-derived cardiomyocytes has to be determined.

Intriguingly, overexpression of 28 out of 2019 miRNAs substantially enhanced cardiomyocyte turnover. Of note, whereas some of the miRNAs that were reported to induce proliferation in murine cardiomyocytes were confirmed in our screening, such as miR-1825 and miR-33b,[8] others did not show a significant proliferative effect

in hiPSC-CM after transient miRNA overexpression, such as miR-590, the miR-302/367 cluster, and the miR-17-92 family.[8,14,15,17] Interestingly, five (miR-515-3p, miR-519e-3p, miR-517c-3p, miR-371a-3p, and miR-371b-3p) out of 28 miRNA candidates from the screening belong to the primate-specific chromosome 19 miR-cluster (C19MC) and adjacent miR-371-373 family, that are expressed predominantly in placental tissue,[21,36,37] and in human embryonic stem cells.[38] As experimental and clinical studies indicate that miRNA members of the C19MC are involved in biological processes related to proliferation, migration, differentiation, extracellular matrix composition, and immunomodulation,[37] we reasoned that these miRNAs are important for cardiomyocyte proliferation due to their involvement of biological processes that comprise key pathways for cardiac regeneration.[39] Notably, the majority of members of the miR-515 and miR-371-373 family tested in the screening did not induce cardiomyocyte turnover, indicating that only a minority of the cluster harvest functional specialization to modulate proliferative pathways in cardiomyocytes.

Indeed, we confirmed that miR-515-3p and miR-519e-3p substantially enhance expression of cell cycling progressors and suppress cell cycling inhibitors. In addition, Aurora B-kinase that is mandatory for cytokinesis was detected in a high number of miR-515-3p and miR-519e-3p-transfected hiPSC-CM and was substantially increased in the midbodies of cardiomyocytes, indicative of cell division. Importantly, transient hypoxia has an additive effect to the proliferative activity observed after miR-515-3p and miR-519e-3p transfection that was not evident in miR-scrambled and miR-371a-3p-treated hiPSC-CM. Interestingly, experimental studies suggest that a distinct population of adult cardiomyocytes maintain their proliferative capacity in a hypoxic environment,[5,6] and activation of cell cycling in cardiomyocytes is more prominent at the border zone of the infarcted myocardium.[40,41] In this regard, miR-515-3p and miR-519e-3p may particularly enhance proliferation in these distinct cardiomyocyte populations. These findings are supported by our RNA-seq that observed enrichment of genes that respond to hypoxia in hiPSC-CM overexpressed with miR-515-3p and miR-519e-3p.

Furthermore, our RNA-seq analysis in miR-515-3p and miR-519e-3p-treated hiPSC-CM reveals downregulation of genes involved in sarcomeric organization, most probably reflecting sarcomeric disassembly that is needed for cell division.[42] In contrast, we observed a strong enrichment of genes that are involved in DNA replication, cell cycle, and cell division, supporting the substantial increase in Aurora B-kinase-positive hiPSC-CM as observed after miR-515-3p and miR-519e-3p-mimic transfection. Indeed, genes of core cardiomyocyte proliferative signaling pathways, such as PI3K-Akt, the WNT/B-catenin, and TGF-B/SMAD, were significantly enriched after miR-515-3p- and miR-519e-3p-mimic transfection. In addition, transcription factors (E2F family (E2F1, E2F2, and E2F7), FOXM1, MYBL1, and MYBL2 (alias B-Myb)) that are master regulators of genes regulating mitosis and cytokinesis[43–46] were substantially upregulated upon miR-mimic transfection. Interestingly, these transcription factors are downregulated in adult cardiomyocytes and after binucleation and fail to be reactivated in mature cardiomyocytes upon myocardial infarction,[43,45] suggesting that miRNA-mediated activation may re-initiate adult cardiomyocyte cell cycle reentry. Conclusively, these observations indicate that induction of proliferation is not dependent on single gene regulation, but rather on modulation of large gene networks that are cooperatively regulated by miR-515-3p and miR-519e-3p.

In summary, our findings on molecular level, together with our functional data, strongly suggest that miR-515-3p and miR-519e-3p are effective for induction of cell cycle reentry and increase cell division in human-derived cardiomyocytes in a timely controlled manner.

Limitations of the study

This study provides a translational perspective to investigate miRNA-mimics derived from the high-throughput screening in pre-clinical models for assessment of miRNA-induced repair and regenerative potential. However, we are aware of the inherent limitations of hiPSC-CM technology used in this study. Notably, hiPSC-CM were cultured for 50 to 60 days to achieve a certain degree of maturation of hiPSC-CM.[47] However, it has to be acknowledged that hiPSC-CM comprise an immature phenotype that share similarities with fetal rather than adult cardiomyocytes,[47] which may also endorse a higher susceptibility to undergo proliferation after miRNA treatment. Therefore, whether application of these miRNAs in adult working cardiomyocytes *in vivo* results in cardiac repair processes will require further investigation. Secondarily, we did not investigate direct targets of miRNAs that contribute to the observed induction of cell division in hiPSC-CMs. Further studies are needed to evaluate specific molecular mechanisms involved in miRNA-induced activation of the cell cycling program in hiPSC-CM.

Conclusions

We explored proliferative potential of more than two thousand miRNAs upon overexpression and inhibition in hiPSC-CM after transient hypoxia. Importantly, efficient induction of cell cycling was restricted to overexpression of miRNAs. Primate-specific miR-515-3p and miR-519e-3p enhanced proliferation in hiPSC-CM through downregulation of pathways involved in sarcomere organization and upregulation of gene networks involved in cell division that is supported by substantial increase in proliferation using immune staining for early and late mitosis markers. Therefore, these miRNAs have the therapeutic potential for cardiac repair in patients with myocardial injury due to transient hypoxia, such as present in myocardial infarction.

STAR★METHODS

Detailed methods are provided in the online version of this paper and include the following:

- KEY RESOURCES TABLE
- RESOURCE AVAILABILITY
  - Lead contact
  - Materials availability
  - Data and code availability
- EXPERIMENTAL MODEL AND SUBJECT DETAILS
  - Cell lines
- METHODS DETAILS
  - Generation of hiPSC-CM
  - HiPSC-CM selection and culture
  - miRNA and siRNA transfection of hiPSC-CM
  - Immunocytochemistry
  - Functional high-throughput screening
  - High content imaging and image analysis of hiPSC-CM
  - High-throughput screening data analysis of hiPSC-CM
  - RNA extraction from hiPSC-CM
  - Reverse transcription (cDNA synthesis) and quantitative real-time PCR (qRT-PCR)
  - RNA sequencing
  - Western blotting
  - Lactate dehydrogenase (LDH) cytotoxicity assay
- QUANTIFICATION AND STATISTICAL ANALYSIS

SUPPLEMENTAL INFORMATION

Supplemental information can be found online at https://doi.org/10.1016/j.isci.2023.106593.

ACKNOWLEDGMENTS

The authors specially thank Sabrina Kleissle from Max Delbrück Center for Molecular Medicine (MDC, Berlin, Germany) as well as Johanna Heine and Sandra Georgi from University Medicine Goettingen for their excellent technical support and Marc Wippich from the Screening Unit at Leibniz-Institute for Molecular Pharmacology (FMP, Berlin, Germany) for high-throughput screening data analysis. This work was supported by the DZHK (German Center for Cardiovascular Research) and the BMBF (German Ministry of Education and Research) (B15-066), Germany (Drs. Jakob, Landmesser and Streckfuss-Bömeke); German Heart Foundation/German Foundation of Heart Research (DSHF, F/37/16, Dr. Jakob); Bayer HealthCare (Grant4targets), Germany; OPO-Foundation, Switzerland; Swiss Heart Foundation (FF21100), Switzerland; Kurt und Senta Herrmann Foundation, Liechtenstein (all to Dr. Jakob). Dr. Jakob was supported by Berlin Institute of Health (BIH) as part of the Clinician Scientist Program. Dr. Renikunta was supported from Berlin-Brandenburg School for Regenerative Therapies as part of the doctoral (Ph.D.) program. Drs. Jakob, Renikunta, and Landmesser are listed as co-inventors on a pending patent held by Charité – University Medicine Berlin that relates to the miRNAs described in this paper for cardiac repair and clinical use. All other authors have reported that they have no relationships relevant to the contents of this paper to disclose.

AUTHOR CONTRIBUTIONS

P.J., H.V.R., and U.L. designed the study. P.J. supervised the study. P.J. and H.V.R. designed and performed experiments. V.N. performed western blots for the study. K.S.B. generated hiPSC-derived cardiomyocytes. K.L. and J.P.V.K. performed high-throughput screening, image acquisition, and data analysis. L.O. performed analysis and interpretation of RNA-seq. H.G., A.K., P.C.S., F.P., S.C., and Y.G. were involved in data interpretation and analysis. F.B.E. and A.H. contributed to data interpretation. P.J. and H.V.R. wrote the manuscript. All authors discussed the results and commented on the manuscript.

DECLARATION OF INTERESTS

The authors P.J., H.V.R., and U.L. are listed as co-inventors on a pending patent held by Charité – University Medicine Berlin that relates to the miRNAs described in this paper for cardiac repair processes.

INCLUSION AND DIVERSITY

We support inclusive, diverse, and equitable conduct of research.

Received: September 6, 2022
Revised: January 7, 2023
Accepted: March 31, 2023
Published: April 8, 2023

REFERENCES

1. Townsend, N., Nichols, M., Scarborough, P., and Rayner, M. (2015). Cardiovascular disease in Europe–epidemiological update 2015. Eur. Heart J. *36*, 2696–2705. https://doi.org/10.1093/eurheartj/ehv428.

2. Bergmann, O., Bhardwaj, R.D., Bernard, S., Zdunek, S., Barnabé-Heider, F., Walsh, S., Zupicich, J., Alkass, K., Buchholz, B.A., Druid, H., et al. (2009). Evidence for cardiomyocyte renewal in humans. Science *324*, 98–102. https://doi.org/10.1126/science.1164680.

3. Porrello, E.R., Mahmoud, A.I., Simpson, E., Hill, J.A., Richardson, J.A., Olson, E.N., and Sadek, H.A. (2011). Transient regenerative potential of the neonatal mouse heart. Science *331*, 1078–1080. https://doi.org/10.1126/science.1200708.

4. Mollova, M., Bersell, K., Walsh, S., Savla, J., Das, L.T., Park, S.Y., Silberstein, L.E., Dos Remedios, C.G., Graham, D., Colan, S., and Kühn, B. (2013). Cardiomyocyte proliferation contributes to heart growth in young humans. Proc. Natl. Acad. Sci. USA *110*, 1446–1451. https://doi.org/10.1073/pnas.1214608110.

5. Nakada, Y., Canseco, D.C., Thet, S., Abdisalaam, S., Asaithamby, A., Santos, C.X., Shah, A.M., Zhang, H., Faber, J.E., Kinter, M.T., et al. (2017). Hypoxia induces heart regeneration in adult mice. Nature *541*, 222–227. https://doi.org/10.1038/nature20173.

6. Kimura, W., Xiao, F., Canseco, D.C., Muralidhar, S., Thet, S., Zhang, H.M., Abderrahman, Y., Chen, R., Garcia, J.A., Shelton, J.M., et al. (2015). Hypoxia fate mapping identifies cycling cardiomyocytes in the adult heart. Nature *523*, 226–230. https://doi.org/10.1038/nature14582.

7. Gabisonia, K., Prosdocimo, G., Aquaro, G.D., Carlucci, L., Zentilin, L., Secco, I., Ali, H., Braga, L., Gorgodze, N., Bernini, F., et al. (2019). MicroRNA therapy stimulates uncontrolled cardiac repair after myocardial infarction in pigs. Nature *569*, 418–422. https://doi.org/10.1038/s41586-019-1191-6.

8. Eulalio, A., Mano, M., Dal Ferro, M., Zentilin, L., Sinagra, G., Zacchigna, S., and Giacca, M. (2012). Functional screening identifies miRNAs inducing cardiac regeneration. Nature *492*, 376–381. https://doi.org/10.1038/nature11739.

9. Diez-Cuñado, M., Wei, K., Bushway, P.J., Maurya, M.R., Perera, R., Subramaniam, S., Ruiz-Lozano, P., and Mercola, M. (2018). miRNAs that induce human cardiomyocyte proliferation converge on the Hippo pathway. Cell Rep. *23*, 2168–2174. https://doi.org/10.1016/j.celrep.2018.04.049.

10. Yang, Y., Cheng, H.-W., Qiu, Y., Dupee, D., Noonan, M., Lin, Y.-D., Fisch, S., Unno, K., Sereti, K.-I., and Liao, R. (2015). MicroRNA-34a plays a key role in cardiac repair and regeneration following myocardial infarction. Circ. Res. *117*, 450–459. https://doi.org/10.1161/CIRCRESAHA.117.305962.

11. Porrello, E.R., Mahmoud, A.I., Simpson, E., Johnson, B.A., Grinsfelder, D., Canseco, D., Mammen, P.P., Rothermel, B.A., Olson, E.N., and Sadek, H.A. (2013). Regulation of neonatal and adult mammalian heart regeneration by the miR-15 family. Proc. Natl. Acad. Sci. USA *110*, 187–192. https://doi.org/10.1073/pnas.1208863110.

12. Porrello, E.R., Johnson, B.A., Aurora, A.B., Simpson, E., Nam, Y.J., Matkovich, S.J., Dorn, G.W., 2nd, van Rooij, E., and Olson, E.N. (2011). MiR-15 family regulates postnatal mitotic arrest of cardiomyocytes. Circ. Res. *109*, 670–679. https://doi.org/10.1161/circresaha.111.248880.

13. Aguirre, A., Montserrat, N., Zacchigna, S., Nivet, E., Hishida, T., Krause, M.N., Kurian, L., Ocampo, A., Vazquez-Ferrer, E., Rodriguez-Esteban, C., et al. (2014). In vivo activation of a conserved microRNA program induces mammalian heart regeneration. Cell Stem Cell *15*, 589–604. https://doi.org/10.1016/j.stem.2014.10.003.

14. Chen, J., Huang, Z.P., Seok, H.Y., Ding, J., Kataoka, M., Zhang, Z., Hu, X., Wang, G., Lin, Z., Wang, S., et al. (2013). mir-17-92 cluster is required for and sufficient to induce cardiomyocyte proliferation in postnatal and adult hearts. Circ. Res. *112*, 1557–1566. https://doi.org/10.1161/circresaha.112.300658.

15. Gao, F., Kataoka, M., Liu, N., Liang, T., Huang, Z.P., Gu, F., Ding, J., Liu, J., Zhang, F., Ma, Q., et al. (2019). Therapeutic role of miR-19a/19b in cardiac regeneration and protection from myocardial infarction. Nat. Commun. *10*, 1802. https://doi.org/10.1038/s41467-019-09530-1.

16. Borden, A., Kurian, J., Nickoloff, E., Yang, Y., Troupes, C.D., Ibetti, J., Lucchese, A.M., Gao, E., Mohsin, S., Koch, W.J., et al. (2019). Transient introduction of miR-294 in the heart promotes cardiomyocyte cell cycle reentry after injury. Circ. Res. *125*, 14–25. https://doi.org/10.1161/circresaha.118.314223.

17. Tian, Y., Liu, Y., Wang, T., Zhou, N., Kong, J., Chen, L., Snitow, M., Morley, M., Li, D., Petrenko, N., et al. (2015). A microRNA-Hippo pathway that promotes cardiomyocyte proliferation and cardiac regeneration in mice. Sci. Transl. Med. *7*, 279ra38. https://doi.org/10.1126/scitranslmed.3010841.

18. Lesizza, P., Prosdocimo, G., Martinelli, V., Sinagra, G., Zacchigna, S., and Giacca, M. (2017). Single-dose intracardiac injection of pro-regenerative MicroRNAs improves cardiac function after myocardial infarction. Circ. Res. *120*, 1298–1304. https://doi.org/10.1161/circresaha.116.309589.

19. Bentwich, I., Avniel, A., Karov, Y., Aharonov, R., Gilad, S., Barad, O., Barzilai, A., Einat, P., Einav, U., Meiri, E., et al. (2005). Identification of hundreds of conserved and nonconserved human microRNAs. Nat. Genet. *37*, 766–770. https://doi.org/10.1038/ng1590.

20. Noguer-Dance, M., Abu-Amero, S., Al-Khtib, M., Lefèvre, A., Coullin, P., Moore, G.E., and Cavaillé, J. (2010). The primate-specific microRNA gene cluster (C19MC) is imprinted in the placenta. Hum. Mol. Genet. *19*, 3566–3582. https://doi.org/10.1093/hmg/ddq272.

21. Ludwig, N., Leidinger, P., Becker, K., Backes, C., Fehlmann, T., Pallasch, C., Rheinheimer, S., Meder, B., Stähler, C., Meese, E., and Keller, A. (2016). Distribution of miRNA expression across human tissues. Nucleic Acids Res. *44*, 3865–3877. https://doi.org/10.1093/nar/gkw116.

22. Bortolin-Cavaillé, M.L., Dance, M., Weber, M., and Cavaillé, J. (2009). C19MC microRNAs are processed from introns of large Pol-II, non-protein-coding transcripts. Nucleic Acids Res. *37*, 3464–3473. https://doi.org/10.1093/nar/gkp205.

23. Zhang, M., Muralimanoharan, S., Wortman, A.C., and Mendelson, C.R. (2016). Primate-specific miR-515 family members inhibit key genes in human trophoblast differentiation and are upregulated in preeclampsia. Proc. Natl. Acad. Sci. USA *113*. E7069-7076. https://doi.org/10.1073/pnas.1607849113.

24. Donker, R.B., Mouillet, J.F., Chu, T., Hubel, C.A., Stolz, D.B., Morelli, A.E., and Sadovsky, Y. (2012). The expression profile of C19MC microRNAs in primary human trophoblast cells and exosomes. Mol. Hum. Reprod. *18*, 417–424. https://doi.org/10.1093/molehr/gas013.

25. Wu, S., Huang, S., Ding, J., Zhao, Y., Liang, L., Liu, T., Zhan, R., and He, X. (2010). Multiple microRNAs modulate p21Cip1/Waf1 expression by directly targeting its 3′ untranslated region. Oncogene *29*, 2302–2308. https://doi.org/10.1038/onc.2010.34.

26. Pagano, M., Pepperkok, R., Verde, F., Ansorge, W., and Draetta, G. (1992). Cyclin A is required at two points in the human cell cycle. EMBO J. *11*, 961–971.

27. Shapiro, S.D., Ranjan, A.K., Kawase, Y., Cheng, R.K., Kara, R.J., Bhattacharya, R., Guzman-Martinez, G., Sanz, J., Garcia, M.J., and Chaudhry, H.W. (2014). Cyclin A2 induces cardiac regeneration after myocardial infarction through cytokinesis of adult cardiomyocytes. Sci. Transl. Med. *6*, 224ra27. https://doi.org/10.1126/scitranslmed.3007668.

28. Bicknell, K.A., Coxon, C.H., and Brooks, G. (2004). Forced expression of the cyclin B1-CDC2 complex induces proliferation in adult rat cardiomyocytes. Biochem. J. *382*, 411–416. https://doi.org/10.1042/bj20031481.

29. Mohamed, T.M.A., Ang, Y.S., Radzinsky, E., Zhou, P., Huang, Y., Elfenbein, A., Foley, A., Magnitsky, S., and Srivastava, D. (2018). Regulation of cell cycle to stimulate adult cardiomyocyte proliferation and cardiac regeneration. Cell *173*, 104–116.e12. https://doi.org/10.1016/j.cell.2018.02.014.

30. Hassink, R.J., Pasumarthi, K.B., Nakajima, H., Rubart, M., Soonpaa, M.H., de la Rivière, A.B., Doevendans, P.A., and Field, L.J. (2008). Cardiomyocyte cell cycle activation improves cardiac function after myocardial infarction. Cardiovasc. Res. *78*, 18–25. https://doi.org/10.1093/cvr/cvm101.

31. Pasumarthi, K.B.S., Nakajima, H., Nakajima, H.O., Soonpaa, M.H., and Field, L.J. (2005). Targeted expression of cyclin D2 results in cardiomyocyte DNA synthesis and infarct regression in transgenic mice. Circ. Res. *96*, 110–118. https://doi.org/10.1161/01.Res.0000152326.91223.4f.

32. Schneider, J.W., Gu, W., Zhu, L., Mahdavi, V., and Nadal-Ginard, B. (1994). Reversal of terminal differentiation mediated by p107 in Rb-/- muscle cells. Science *264*, 1467–1471. https://doi.org/10.1126/science.8197461.

33. MacLellan, W.R., Garcia, A., Oh, H., Frenkel, P., Jordan, M.C., Roos, K.P., and Schneider, M.D. (2005). Overlapping roles of pocket proteins in the myocardium are unmasked by germ line deletion of p130 plus heart-specific deletion of Rb. Mol. Cell Biol. *25*, 2486–2497. https://doi.org/10.1128/MCB.25.6.2486-2497.2005.

34. Scalise, M., Marino, F., Salerno, L., Mancuso, T., Cappetta, D., Barone, A., Parrotta, E.I., Torella, A., Palumbo, D., Veltri, P., et al. (2021). In vitro CSC-derived cardiomyocytes exhibit the typical microRNA-mRNA blueprint of endogenous cardiomyocytes. Commun. Biol. *4*, 1146. https://doi.org/10.1038/s42003-021-02677-y.

35. Senyo, S.E., Steinhauser, M.L., Pizzimenti, C.L., Yang, V.K., Cai, L., Wang, M., Wu, T.D., Guerquin-Kern, J.L., Lechene, C.P., and Lee, R.T. (2013). Mammalian heart renewal by pre-existing cardiomyocytes. Nature *493*, 433–436. https://doi.org/10.1038/nature11682.

36. de Rie, D., Abugessaisa, I., Alam, T., Arner, E., Arner, P., Ashoor, H., Åström, G., Babina, M., Bertin, N., Burroughs, A.M., et al. (2017). An integrated expression atlas of miRNAs and their promoters in human and mouse. Nat. Biotechnol. *35*, 872–878. https://doi.org/10.1038/nbt.3947.

37. Mouillet, J.F., Goff, J., Sadovsky, E., Sun, H., Parks, T., Chu, T., and Sadovsky, Y. (2020). Transgenic expression of human C19MC miRNAs impacts placental morphogenesis. Placenta *101*, 208–214. https://doi.org/10.1016/j.placenta.2020.09.069.

38. Ren, J., Jin, P., Wang, E., Marincola, F.M., and Stroncek, D.F. (2009). MicroRNA and gene expression patterns in the differentiation of human embryonic stem cells. J. Transl. Med. *7*, 20. https://doi.org/10.1186/1479-5876-7-20.

39. Sereti, K.I., Nguyen, N.B., Kamran, P., Zhao, P., Ranjbarvaziri, S., Park, S., Sabri, S., Engel, J.L., Sung, K., Kulkarni, R.P., et al. (2018). Analysis of cardiomyocyte clonal expansion during mouse heart development and injury. Nat. Commun. *9*, 754. https://doi.org/10.1038/s41467-018-02891-z.

40. Eschenhagen, T., Bolli, R., Braun, T., Field, L.J., Fleischmann, B.K., Frisén, J., Giacca, M., Hare, J.M., Houser, S., Lee, R.T., et al. (2017). Cardiomyocyte regeneration: a consensus statement. Circulation *136*, 680–686. https://doi.org/10.1161/circulationaha.117.029343.

41. Hsieh, P.C.H., Segers, V.F.M., Davis, M.E., MacGillivray, C., Gannon, J., Molkentin, J.D., Robbins, J., and Lee, R.T. (2007). Evidence from a genetic fate-mapping study that stem cells refresh adult mammalian cardiomyocytes after injury. Nat. Med. *13*, 970–974. https://doi.org/10.1038/nm1618.

42. Jopling, C., Sleep, E., Raya, M., Martí, M., Raya, A., and Izpisúa Belmonte, J.C. (2010). Zebrafish heart regeneration occurs by cardiomyocyte dedifferentiation and proliferation. Nature *464*, 606–609. https://doi.org/10.1038/nature08899.

43. Windmueller, R., Leach, J.P., Babu, A., Zhou, S., Morley, M.P., Wakabayashi, A., Petrenko, N.B., Viatour, P., and Morrisey, E.E. (2020). Direct comparison of mononucleated and binucleated cardiomyocytes reveals molecular mechanisms underlying distinct proliferative competencies. Cell Rep. *30*, 3105–3116.e4. https://doi.org/10.1016/j.celrep.2020.02.034.

44. Ebelt, H., Zhang, Y., Kampke, A., Xu, J., Schlitt, A., Buerke, M., Müller-Werdan, U., Werdan, K., and Braun, T. (2008). E2F2 expression induces proliferation of terminally differentiated cardiomyocytes in vivo. Cardiovasc. Res. *80*, 219–226. https://doi.org/10.1093/cvr/cvn194.

45. Quaife-Ryan, G.A., Sim, C.B., Ziemann, M., Kaspi, A., Rafehi, H., Ramialison, M., El-Osta, A., Hudson, J.E., and Porrello, E.R. (2017). Multicellular transcriptional analysis of mammalian heart regeneration. Circulation *136*, 1123–1139. https://doi.org/10.1161/CIRCULATIONAHA.117.028252.

46. Gründl, M., Walz, S., Hauf, L., Schwab, M., Werner, K.M., Spahr, S., Schulte, C., Maric, H.M., Ade, C.P., and Gaubatz, S. (2020). Interaction of YAP with the Myb-MuvB (MMB) complex defines a transcriptional program to promote the proliferation of cardiomyocytes. PLoS Genet. *16*, e1008818. https://doi.org/10.1371/journal.pgen.1008818.

47. Karbassi, E., Fenix, A., Marchiano, S., Muraoka, N., Nakamura, K., Yang, X., and Murry, C.E. (2020). Cardiomyocyte maturation: advances in knowledge and implications for regenerative medicine. Nat. Rev. Cardiol. *17*, 341–359. https://doi.org/10.1038/s41569-019-0331-x.

48. Borchert, T., Hübscher, D., Guessoum, C.I., Lam, T.D.D., Ghadri, J.R., Schellinger, I.N., Tiburcy, M., Liaw, N.Y., Li, Y., Haas, J., et al. (2017). Catecholamine-dependent beta-adrenergic signaling in a pluripotent stem cell model of takotsubo cardiomyopathy. J. Am. Coll. Cardiol. *70*, 975–991. https://doi.org/10.1016/j.jacc.2017.06.061.

49. Streckfuss-Bömeke, K., Wolf, F., Azizian, A., Stauske, M., Tiburcy, M., Wagner, S.,

Hübscher, D., Dressel, R., Chen, S., Jende, J., et al. (2013). Comparative study of human-induced pluripotent stem cells derived from bone marrow cells, hair keratinocytes, and skin fibroblasts. Eur. Heart J. *34*, 2618–2629. https://doi.org/10.1093/eurheartj/ehs203.

50. Magadum, A., Ding, Y., He, L., Kim, T., Vasudevarao, M.D., Long, Q., Yang, K., Wickramasinghe, N., Renikunta, H.V., Dubois, N., et al. (2017). Live cell screening platform identifies PPARdelta as a regulator of cardiomyocyte proliferation and cardiac repair. Cell Res. *27*, 1002–1019. https://doi.org/10.1038/cr.2017.84.

51. Magadum, A., Renikunta, H.V., Singh, N., Estaras, C., Kishore, R., and Engel, F.B. (2022). Live cell screening identifies glycosides as enhancers of cardiomyocyte cell cycle activity. Front. Cardiovasc. Med. *9*, 901396. https://doi.org/10.3389/fcvm.2022.901396.

52. Livak, K.J., and Schmittgen, T.D. (2001). Analysis of relative gene expression data using real-time quantitative PCR and the 2(-Delta Delta C(T)) Method. Methods *25*, 402–408. https://doi.org/10.1006/meth.2001.1262.

STAR★METHODS

KEY RESOURCES TABLE

REAGENT or RESOURCE	SOURCE	IDENTIFIER
Antibodies		
Mouse Monoclonal Anti- AIM-1(Aurora B)	BD Biosciences	Cat #611082
Mouse Monoclonal Anti-Sarcomeric Alpha Actinin	Abcam	Cat #Ab9465
Mouse Monoclonal Human Troponin T (Cardiac)	R & D Systems	Cat #MAB-1874
Goat Polyclonal Anti-Cardiac Troponin I	Abcam	Cat #Ab56357
Rabbit Polyclonal Anti-phospho-Histone-H3 (Ser10)	Merck Millipore	Cat #06-750
Rabbit Monoclonal P21 (CDKN1A)	Thermo Fisher Scientific	Cat #MA5-14949
Mouse Monoclonal Anti- Cyclin A2 (CCNA2)	Abcam	Cat #AB16726
chicken polyclonal Anti- GAPDH	Merck Millipore	Cat #AB2302
Anti-Rabbit IgG, HRP-Linked	Cell signaling	Ca t#7074
Anti-Mouse IgG, HRP-Linked	Cell signaling	Cat #7076
anti-Chicken IgG, HRP-Linked	Santa Cruz	Cat #SC-2428
Goat anti-Mouse (Alexa 488)	Thermo Fisher Scientific	Cat #A-11001
Goat anti-Rabbit (Alexa 488)	Thermo Fisher Scientific	Cat #A-11008
Goat anti-Rabbit (DyLight 488)	Thermo Fisher Scientific	Cat #35552
Goat anti-Mouse (Alexa 594)	Thermo Fisher Scientific	Cat #A-11032
Goat anti-Rabbit (Alexa 594)	Thermo Fisher Scientific	Cat #A-11012
Donkey anti-Mouse (Alexa 488)	Thermo Fisher Scientific	Cat #A-21202
Donkey anti-Rabbit (Alexa 488)	Thermo Fisher Scientific	Cat # A-21206
Donkey anti-Mouse (Alexa 594)	Thermo Fisher Scientific	Cat #A-21203
Donkey anti-Rabbit (Alexa 594)	Thermo Fisher Scientific	Cat #A-21207
Bacterial and virus strains		
	This Paper	N/A
	This Paper	N/A
Biological samples		
	This Paper	N/A
	This Paper	N/A
Chemicals, peptides, and recombinant proteins		
RPMI 1640 mit HEPES mit GlutaMAX	Thermo Fisher Scientific	Cat #72400021
B27 Insulin (Serum Free) (10 mL) (50X)	Thermo Fisher Scientific	Cat #17504044
Geltrex (Growth Factor Reduced)	Thermo Fisher Scientific	Cat #A1413302
Trypsin/EDTA (0, 25%/0, 02%)	Merck Millipore	Cat #L2163
Stem pro Accutase cell Dissociation reagent	Thermo Fisher Scientific	Cat #A11105-01
Fetal Bovine Serum, SAFC, (FBS)	Sigma-Aldrich	Cat #12103C
Thiazovivin (2 µM final)	Merck Millipore	Cat # 420220
Collagenase CLS-2 (1 g)	Worthington	Cat # LS004176
DMEM/F-12, HEPES (500 mL)	Thermo Fisher Scientific	Cat #113300-32
RPMI 1640 Medium (ATCC modification)	Thermo Fisher Scientific	Cat # A10491-01
Critical commercial assays		
miRNeasy Micro Kit	Qiagen	Cat #217084
CyQUANT LDH Cytotoxicity Assay Kit, fluorescence	Thermo Fisher Scientific	Cat #C20301

(*Continued on next page*)

Continued

REAGENT or RESOURCE	SOURCE	IDENTIFIER
Click-iT EdU Plus Cell Proliferation Kit (Alexa 488)	Thermo Fisher Scientific	Cat #C10637
Click-iT EdU Plus Cell Proliferation Kit (Alexa 594)	Thermo Fisher Scientific	Cat #C10639
BCA-Protein Assay Kit	Thermo Fisher Scientific	Cat #23225
Supersignal westDura Extended	Thermo Fisher Scientific	Cat #34076
High-capacity cDNA Reverse Transcription kit	Thermo Fisher Scientific	Cat #4368814
TaqMan miRNA reverse transcription kit	Thermo Fisher Scientific	Cat #4366596
TaqMan miRNA fast advanced master mix	Thermo Fisher Scientific	Cat #4444557
4-20% pre-cast Protein Gels	Bio-Rad	Cat #4561096
Deposited data		
RNA-Sequencing data	This Paper	ENA: PRJEB44561
Experimental models: Cell lines		
WTD2- hiPSC cardiomyocytes	University Medical Center Göttingen	N/A
Control 1- hiPSC cardiomyocytes	University Medical Center Göttingen	N/A
Experimental models: Organisms/strains		
	This Paper	N/A
	This Paper	N/A
Oligonucleotides		
List of Human primers used for qRT-PCR are in Table S7	This Paper	N/A
Human mirVana miRNA-mimics		
miRNA Mimic, Negative Control #1	Thermo Fisher Scientific	Cat # 4464058
hsa-miR-1825	Thermo Fisher Scientific	Cat # MC13549
hsa-miR-515-3p	Thermo Fisher Scientific	Cat # MC12885
hsa-miR-519e-3p	Thermo Fisher Scientific	Cat # MC13103
hsa-miR-371a-3p	Thermo Fisher Scientific	Cat #MC12262
Human mirVana miRNA-inhibitors		
Anti-miR-99-5p	Thermo Fisher Scientific	Cat # MH10719
Anti-miR-100-5p	Thermo Fisher Scientific	Cat # MH10188
Anti-miR-195-5p	Thermo Fisher Scientific	Cat # MH10827
Human microRNA- TaqMan Primers		
RNU48	Thermo Fisher Scientific	Assay id #001006
hsa-miR-195-3p	Thermo Fisher Scientific	Assay id #000494
Recombinant DNA		
	This Paper	N/A
	This Paper	N/A
Software and algorithms		
GraphPad Prism version 7.0	Graphpad	N/A
ThermoScientific HCS Studio, Cell-omics	Cellomics	N/A
ImageJ	NIH	N/A
Columbus Image Data Storage and Analysis System	PerkinElmer	N/A
KNIME Analytics Platform	KNIME	N/A
Other		
	This Paper	N/A

RESOURCE AVAILABILITY

Lead contact

Further information and requests for resources and reagents should be directed to and will be fulfilled by the lead contact, Philipp Jakob, MD (Philipp.jakob@usz.ch).

Materials availability

This study did not generate new unique reagents.

Data and code availability

- RNA-Sequencing data is deposited in the ENA database and are publicly available as of the date of publication. Accession numbers are listed in the key resources table.
- This paper does not report original code.
- Any additional information required to reanalyze the data reported in this paper is available from the lead contact upon request.

EXPERIMENTAL MODEL AND SUBJECT DETAILS

Cell lines

Human induced pluripotent cell (hiPSC) derived Cardiomyocytes (hiPSC-CMs; WTD2 and Control 1) were obtained from University Medical Center Göttingen, Germany. Two Cell lines were generated with an episomal plasmid-based transduction. One female and one male hiPSC line was reprogrammed with the STEMCCA system, which is a humanized excisable lentiviral system containing all four reprogramming factors OCT4, SOX2, KLF4, and c-MYC in a single "stem cell cassette" (pHAGE2-EF1aFull-hOct4-F2A-hKlf4-IRES-hSox2-P2A-hcMyc-W-loxP). The pluripotent clones were expanded up to passage 8. HiPSCs were effectively differentiated and selected *in vitro* into >90% pure cardiomyocytes. Fifty to 60 or 110 to 120 days old hiPSC-CM were used for experiments.

METHODS DETAILS

Generation of hiPSC-CM

As model system, human induced pluripotent stem cell (hiPSC)-derived cardiomyocytes (CMs) (hiPSC-CM) were used. HiPSCs were generated as previously described.[48,49] Female and male donors were used to generate cardiomyocytes, with two different reprogramming-based approaches. Two female hiPSC lines were generated with an episomal plasmid-based transduction. One female and one male hiPSC line was reprogrammed with the STEMCCA system, which is a humanized excisable lentiviral system containing all four reprogramming factors OCT4, SOX2, KLF4, and c-MYC in a single "stem cell cassette" (pHAGE2-EF1aFull-hOct4-F2A-hKlf4-IRES-hSox2-P2A-hcMyc-W-loxP). The pluripotent clones were expanded up to passage 8. The established iPSCs were proven for their pluripotency by both *in vitro* studies - the expression of pluripotency markers and differentiation experiments - and *in vivo* teratoma formation assay. All protocols were approved by the Ethics Committee of the University Medical Center Göttingen (No. 10/9/15). Informed consent was obtained from all participants and all research was performed in accordance with relevant guidelines and regulations and in accordance with the Declaration of Helsinki.

HiPSC-CM selection and culture

Post differentiation, cardiac culture medium (RPME 1640 with Glutamax and HEPES, B27 supplement) was aspirated and replaced with cardio selection medium (RPMI 1640 without Glucose, Lactate/HEPES, hAlbumin, human recombinant L-Ascorbic Acid 2-Phosphate). The medium was exchanged every second day. Post selection, the medium was replaced with cardiac culture medium. HiPSCs were effectively differentiated and selected *in vitro* into >90% pure cardiomyocytes. Fifty to 60 or 110 to 120 days old hiPSC-CM were used for experiments. Cell detachment was performed using 0.25% trypsin, 0.02% EDTA and Stempro accutase, followed by collagenase diluted in RPME 1640 for cell dissociation. Thereafter, cells were seeded in cardio digestion medium (RPME 1640 with Glutamax and HEPES, B27 Supplement, 10% FBS, Thiazovivin (2 μM)). Medium was replaced to cardiac culture medium 48 h later. Cell culture plates were coated with Geltrex.

miRNA and siRNA transfection of hiPSC-CM

Lullaby stem (OZ Biosciences) was used for transfection of miRNAs using a standard forward transfection protocol. Medium was replaced with fresh cardiac culture medium 24 h post transfection. 48 h post transfection, hiPSC-CM were exposed to hypoxia (0.5% oxygen, 5% CO2) for 2 h. Thereafter, medium was exchanged to cardio culture medium containing EdU, or hiPSC-CM were fixed and stained with H3P or Aurora B-kinase and further proceeded for immunocytochemistry. Assessment of FAM-miR transfected hiPSC-CM was performed 24 h post transfection using fluorescent imaging or fluorescence-activated cell sorting (FACS). For FACS analysis, cells were briefly washed in PBS, trypsinized, and the detached cells were resuspended with freshly mixed staining solution (100 μL Annexin-biding buffer was added for each sample). The mix was carefully vortexed and incubated for a period of 20 min in dark at 4°C and samples were measured immediately at an Attune flow cytometer. All-stars Hs Cell Death Control siRNA (Qiagen) was used to observe a cell death phenotype in hiPSC-CM 48 h post transfection.

Immunocytochemistry

Staining was performed as previously described.[50,51] HiPSC-CM were washed shortly with PBS and fixed with 3.7% formaldehyde (Sigma). Cells were washed three times with PBS and permeabilized with 0.5% Triton X-100 in PBS, and washed three times in PBS. HiPSC-CM were blocked for 1 h at RT with blocking buffer (10% Horse serum, 1% BSA, 0.3% Triton) in PBS and incubated with primary antibodies in dilution buffer (1x PBS, 1% BSA, 1% donkey or horse serum, 0, 3% Triton) overnight at 4°C. Subsequently, hiPSC-CM were washed three times with 0.1% Nonidet P40 in PBS, and incubated with corresponding secondary antibodies conjugated with Alexa Fluor 488 and Alexa Fluor 594 (1:500 Life technologies) for 1 h at RT. HiPSC-CM were washed three times with 0.1% BSA. EdU incorporation assay was performed by incubating cells with Click it reaction mix cocktail kit (Life Technologies, Invitrogen) for 30 min, according to manufacturer protocol. HiPSC-CM were washed three times with 0.1% BSA in PBS, followed by incubation with respective secondary antibodies for 1 h at RT. HiPSC-CM were later incubated with Hoechst (Nuclear stain) and washed three times with 1xPBS.

Functional high-throughput screening

A high-throughput screening (HTS) by using a miRNA-library (Thermo Fisher Scientific/Ambion; mirVana Human Library v19.0; 2019 miR-mimics and miR-inhibitors) was performed in two individual screenings. Three thousand and five hundred hiPSC-CM/well were plated on Geltrex (Thermo Fisher Scientific) -coated 384-well plates (Corning) using an EL406 washer dispenser (BioTeK) in a laminar flow work cabinet to avoid contamination. For each miRNA, 400 nM dilution of the miRNA were complexed with Lullaby Stem (OZ Biosciences) according to the manufacturer protocol. The mixture was transferred to the 384-well assay plate (Corning) using a Freedom EVO liquid handling workstation (Tecan) resulting in a final concentration of 60 nM miRNA in a total volume of 50 μL per well with a slow dispense speed (1 μL/s). miRNA transfected hiPSC-CM were kept for 24 h at 37°C in 5% CO2. Medium exchange was performed by an EL406 washer dispenser (BioTeK) after 24 h 48 h post transfection, hiPSC-CM were exposed to transient hypoxia (0.5% oxygen, 5% CO2) for 2 h. Thereafter, cells were replaced with cardio culture medium containing EdU and incubated for 48 h. Thereafter, cells were fixed and processed for immunofluorescence analysis.

High content imaging and image analysis of hiPSC-CM

HiPSC-CM were fixed and stained. The immunofluorescence imaging was performed on an ArrayScan XTI High Content Screening Platform (ThermoScientific). 20× magnification objective was used, with a camera mode of 1104x1104 pixel. Three imaging channels were used, Channel 1 was represented as Hoechst (Nucleus marker/Thermo Fisher Scientific), Channel 2 as Troponin T (R&D systems), and Channel 3 as EdU (Thermo fisher scientific). Per well, 36 images from all three channels were acquired from a 384-well plate, covering the majority of the well area. Image analysis was performed with the integrated software, ThermoScientific HCS Studio, cell scan version 6.6.0 (Thermos Fisher Scientific). The first parameter was to identify the cell objects, where the primary object was selected as Channel 1 (Nuclei), later Channel 3 (EdU), as DNA synthesis localizes in the nuclei. Primary Object Identification Mask (Region of Interest = ROI) from Channel 1 (Nuclei) was carried over to Channel 3 without modification. Edu-positive nuclei/cells were selected based on the average intensity in the ROI being >2000. Object selection was based on Channel 1 and Channel 3, as hiPSC-CM were confluent enough for Channel 2. The two used criteria for image output was 1) number of valid objects from nuclei per well and 2) % of EdU-positive objects (nuclei) per well (related to the number of valid objects (nuclei)).

High-throughput screening data analysis of hiPSC-CM

All data was processed using the KNIME analytics platform (KNIME). For plate-wise normalization, the *Z* score for each candidate miRNA on the plate was calculated. A *Z* score was calculated from the % of EdU-positives as follows:

$$Z\ \text{score} = (x - \text{median}(x\ [\text{subset}]))/\text{mad}(x\ [\text{subset}])$$

Where x is the % of EdU-positives in the well, median(x [subset]) is the median from all candidate wells in the plate and mad(x [subset]) the median absolute deviation of all candidate wells in the plate. The mean for the results from the two replicates then was calculated using the following formula: (*Z* score R1+*Z* score R2)/2 and used for the final candidate ranking.

RNA extraction from hiPSC-CM

Total RNA was isolated from hiPSC-CM using the RNeasy Kit (Qiagen). Kits were used according to the manufacturer instructions. HiPSC-CM were seeded and transfected in 24- or 48-well cell culture plates. 48 h and 72 h post microRNA-transfection, cell culture medium was aspirated, and cells were washed three times with sterile DPBS. QIAzol lysis reagent was added onto cells and incubated for 5 min at RT. The resulting cell lysates were collected in 1.5 mL nuclease free reaction tubes (Eppendorf). MiRNeasy RNA extraction kit (Qiagen) was used to isolate the RNA according to the manufacturer instructions. The RNA concentration was measured using Nano drop at 260/280 nm. The isolated RNA was dissolved in 14 μL of RNAse-free water and stored at −80°C or continued for reverse transcription.

Reverse transcription (cDNA synthesis) and quantitative real-time PCR (qRT-PCR)

Gene expression quantification was performed according to standard protocols. The isolated RNA was dissolved in 14 μL of RNAse-free water and stored at −80°C or continued for reverse transcription. High-capacity reverse transcription kit (Thermo Fisher Scientific) for cDNA synthesis was used. SYBR green detection method was used for performing qPCR in 384-well plate and analyzed by Viia R real-time PCR system (Applied Bio systems). Fold changes in gene expression were analyzed by relative quantification by taking means of Ct values of gene of interest and a housekeeping gene (GAPDH) that served as a normalizing control. The fold change was calculated by 2-ΔΔCT formula.[52] For expression of miRNA, RNA was isolated after transfection of hiPSC-CM with hsa-*anti*-miR-195-5p (Thermo Fisher Scientific) as mentioned above. TaqMan microRNA reverse transcription kit was used to perform reverse transcription and TaqMan microRNA fast advanced master mix and TaqMan microRNA primers (Thermo Fisher Scientific) were used. Expression of miR-195-5p was normalized with that of RNU48.

RNA sequencing

MiRNA-scrambled, hsa-miR-mimic-515-3p and hsa-miR-mimic-519e-3p were transfected into hiPSC-CM as described above. 72 h post transfections, cells were washed with DPBS three times. Thereafter QIAzol (Qiagen- MiRNeasy RNA extraction) was added. Resulting lysates were collected in 1.5 mL nuclease free reaction tubes (Eppendorf). RNA-Sequencing was performed by ArrayStar (Arraystar, Inc., USA). Total RNA was used to prepare the sequencing library using KAPA Stranded RNA-Seq Library Prep Kit (Illumina). Libraries were sequenced using HiSeq 4000 (Illumina). Image analysis and base calling was performed using the Solexa pipeline v1.8 (OffLine Base Caller software, v1.8). The raw reads were first cleaned by removing adapter sequences, trimming low quality ends, and filtering reads with low quality (phred quality <20) using Fastp (Version 0.20)). Sequence pseudo alignment of the resulting high-quality reads to the human reference genome (build GRCh38.p13, GENCODE release 32) and quantification of gene level expression was carried out using Kallisto (Version 0.46.1). To detect differentially expressed genes we applied a count based negative binomial model implemented in the software package EdgeR (R version: 4.0.3) using the GLM framework. Genes showing altered expression with adjusted (Benjamini and Hochberg method) p value <0.05 were considered differentially expressed.

Western blotting

HiPSC-CM were transfected with individual miRNAs. HiPSC-CM were lysed with freshly prepared RIPA lysis buffer 72 h post transfection. Cell lysates were collected and centrifuged at 13000 rpm for 20 min at 4°C. Supernatants from centrifugation were collected and the pellet was discarded. BCA protein assay kit (Pierce) was used to determine the protein concentration. Equal amount (40 μg) of proteins were resolved

by 4–20% Pre cast protein gels (Bio-Rad) and blotted onto a polyvinylidene difluoride (PVDF) membrane. Membranes were blocked with 5% Milk or 5% BSA, incubated with primary antibodies over night at 4°C, followed by incubation with HRP-linked secondary antibodies. Chemiluminescent substrate (Supersignal westDura Extended) solution was added onto the membrane and the membrane was developed under chemiluminesence to detect antibody-labeled proteins (INTAS Detection System).

Lactate dehydrogenase (LDH) cytotoxicity assay

LDH assay was performed with the LDH assay kit (Pierce, Thermo Scientific) according to the manufacturer protocols. HiPSC-CM were plated in 96- or 384- well plates, and transfected with either scrambled-miRNA or miRNA-mimics using concentrations ranging from 20 nM to 100 nM to assess toxicity. Medium was carefully collected and placed in a 384-well plate. LDH start reagent was added onto the cells and incubated for a period of 30 min. Thereafter, LDH assay stop solution was added to stop the reaction and measured with a fluorescent plate reader (Tecan) at 490 nm and 690 nm absorbance.

QUANTIFICATION AND STATISTICAL ANALYSIS

Data are presented as means $\pm$ standard error of the mean (SEM). Bars represent average of a minimum of three to five independent experiments with an average of two replicates for each experiment. Data analysis was conducted using Prism 7 Software (Graphpad). We analyzed the data using un-paired Student's t test for single comparisons. One-way or two-way ANOVA (using the post-hoc Tukey or Bonferroni's test) were used for multiple comparisons. A value of $p \leq 0.05$ was considered as statistically significant.